Physics
Department

Walther Meissner
Institute

Bayerische Akademie
der Wissenschaften

Synthesis and Characterization of Iron Arsenic (FeAs) based Superconductors

Master Thesis

Monika Bahurupi

Advisor: Prof. Dr. Rudolf Gross
Garching, March 2009

Technische Universität München

Table of Contents

Chapter 1

1. Introduction

More than 20 years ago, the discovery of High Temperature Superconductivity (HTSC) in copper oxides attracted much attention and led to publication of thousands of experimental and theoretical papers. The recent discovery of superconductivity in the Fe based layered pnictide oxides has sparked immense interest in the chemistry and physics society reminiscent of the discovery of the cuprates superconductors in the mid 1980`s (1986).

On 23rd February, a group from Tokyo Institute of technology published paper in (JACS) Journal of the American society, in which they reported that the fluorine doped lanthanum Oxide Iron Arsenide superconducts at 26 K. [1]. After the publication of this paper within month a Chinese group from Beijing reported that they replaced Lanthanum (La) with Cerium (Ce) and boosted T_c to 41 k. Another group from china replaced Lanthanum (La) with samarium (Sm) and raised T_c to 43 k. By replacing La with rare earth ions of smaller radii the critical temperature increased from 26K in LaOFFeAs to 55K in SmOFFeAs within a couple of days.

Since the discovery of cuprates in 1986 no other material has reached a superconducting transition as high as 55K. The discovery in early 2008 of the new class of high temperature superconductors has broken the monopoly in the cuprates in the physics of high temperature superconducting compounds. At present dozens of HTSC compounds are known to have of superconducting transitions T_c temperatures exceeding 24K. The compounds represented below are some examples of cuprates.

Compound	**Tc**
$HgBa_2Ca_2Cu_3O_8$	134
$Tl_2Ca_2Ba_2Cu_3O_{10}$	127
$Y Ba_2Cu_3O_7$	92
$Bi_2Sr_2CaCu_2O_8$	89
$La_{1.83}Sr_{0.17}CuO_4$	37
$Nd_{1.85}Ce_{0.15}CuO_4$	24

After more than 20 years the cuprates are the most extensively studied class of compounds in condensed matter physics. While superconductivity in conventional metals is well understood by the BCS theory, the mechanism that is responsible for the pairing of carriers in the cuprates is far from being clear. Besides cuprates there are some other superconductors in the HTSC group, which is shown in the following table.

Compound	**Tc**
MgB_2	39
$RbCS_2C_{60}$	33
K_3C_{60}	19
Sr_2RuO_4	1.4

But none of the compounds represented above is a representative of a wide class of compounds like, cuprates and does not reach as high as cuprates in transition temperature. All these compounds were studied in details; in fact research is still going on the cuprates. So up to now there was only the cuprates monopoly in the class of high transition temperature superconductors. But discovery of new iron based superconductors breaks this monopoly.

The undoped LaFeAsO, which is the parent compound to the superconductor, is a member of the large LnTmPnO family. Where Ln represents a 4f rare earth element. Tm- transition metal element with more than half filled 3d shell which consists Mn, Fe, Co, Ni and Pn – pnicogen element. Pnicogens are the group 15 elements of the periodic table. This group consists of nitrogen (N), phosphorus (P), arsenic (As), antimony (Sb), bismuth (Bi). These iron superconductors also refer as "Oxypnictide" oxypnictide are class of materials including oxygen, a pnictogen.

The first superconducting iron oxypnictide was discovered in 2006, based on phosphorus. Such as LaOFeP with 5K and LaONiP with 3K which has not attracted much attention. When phosphorus was substituted by arsenic there was drastic increase in critical temperature. The oxypnictide shows the layered structure like cuprates. They have common ZrCuSiAs type crystal structure belonging to the tetragonal P4/nmm space group. Besides these quaternary REOFeAs (1111) oxypnictide superconductors several high Tc superconductors have been discovered also in other Fe based analogues compounds including ternary compound AFe_2As_2 (A is an alkali earth metal element such as Sr and Ba). By synthesis of $Ba_{1-x}K_xFe_2As_2$ superconductivity was observed with a critical temperature Tc-38K. This compound is known as (122). (The numbers referring to the ratio of the elements in the compound in order of sequence.)

One more type of Fe based superconductor is represented by (111) LiFeAs system where superconductitivity appears at Tc-18K and other simple system is FeSe (Te) (11) system with Tc -8K reaching 27K under pressure of 1.48Gpa. The electronic structure of these systems is more or less similar.

This work presents synthesis and characterization of two types of samples, one is $SmO_{1-x}F_xFeAs$ (1111) and other is oxygen free $Ba_{1-x}K_xFe_2As_2$ (122). Second chapter review the physical properties of this new class of high temperature superconductor. In the third chapter attention is given to the experimental facts use to analyze the electronic structure of this Fe based material. The fourth and fifth chapter will introduce different experimental techniques used to characterize these samples and characterization of these samples.

The work presented here is still suffering from sample related problems.

Chapter 2

2. FeAs based compounds

2.1 Quaternary Rare earth Iron Arsenide (REFeAsO)

REFeAsO constitute a rather small fraction of a much larger family of compounds with the tetragonal ZrCuSiAs type structure belongs to the space group P4/nmm. Pnictide oxides and fluorides chalcogenides-oxides, as well as sillicide and germanide hydrides are among them. Among the pnictide oxides, those with a ZrCuSiAs-type structure have been under intense investigation because of the recent discovery of superconductivity in REFeOP. The equiatomic quaternary pnictide oxides REMPnO, where RE-Rare earth element, actinide; M-transition metal element with a more than half filled 3d shell, and Pn - pnictogen with the ZrCuSiAs type structure, is the largest family of layered d-metal pnictide oxides. These pnictide oxides can be described with the electron precise formula $\mathrm{RE3}^{+}T^{2+}Pn^{3-}\mathrm{O}^{2-}$. The ZrCuSiAs structure has more than 150 representatives. These compounds are composed of two different layers, both with tetrahedral coordination. The crystal structure of ZrCuSiAs type pnictide oxides is shown in the Figure (2.1).

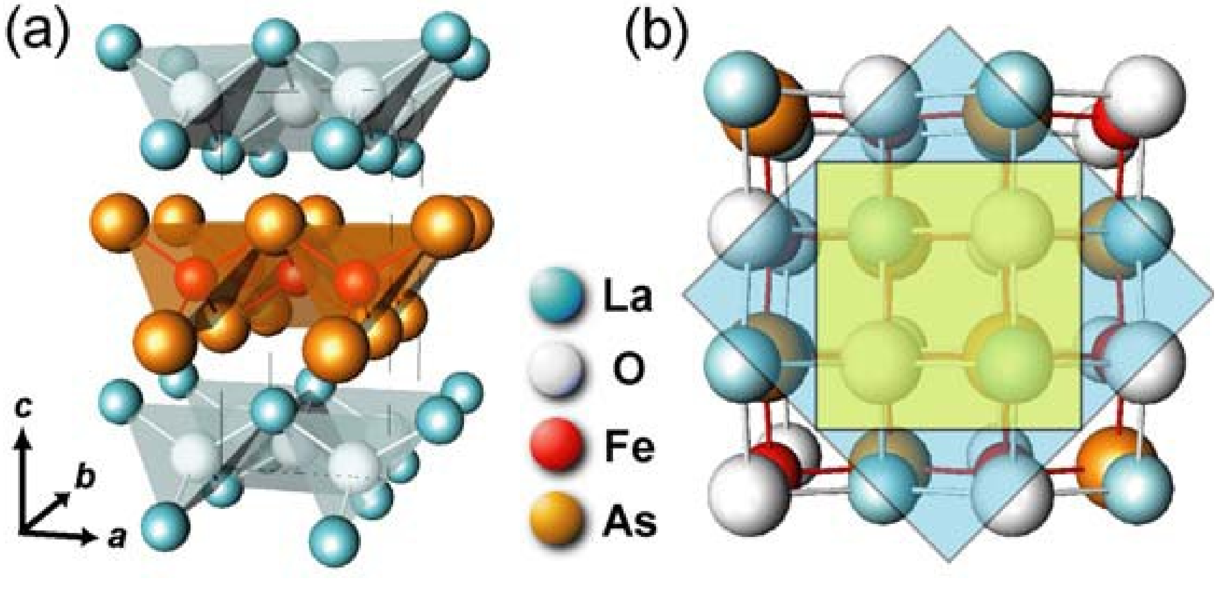

__Figure 2.1:__ Crystal structure of LaFeAsO. (a) The schematic view of the crystal structure demonstrates the layered structure. Distorted tetrahedrons of FeAs$_4$ are connected in an edge sharing manner to form the FeAs layer. (b) Top view of the crystal structure from c-direction. The inner square represents the unit cell in the tetragonal phase (P4/nmm). The outer square is that in the orthorhombic phase (Cmma). [3]

The above structure consists of alternating fluorite type layers (M_2Pn_2) and non fluorite type layers (Ln_2O_2). The fluorite type (M_2Pn_2) layers consists of square nets of M (metal ions) capped with the Pn (pnictogen ions) and alternately above and below the net centers. In this layer the M (metal atoms) are tetrahedrally coordinated by four heavier Pn (pnictogen atoms). The non fluoride type (Ln_2O_2) layer also has the same configuration of atoms, but it is in the reverse manner. O ions are tetrahedrally coordinated by four Ln (rare earth ions). The different tetrahedral layers are stacked in an AB- AB sequence such that they have common layered crystal structure belongs to P4/nmm space group. [39]. As we can see the chemical bonding within the layers are covalent, while the interlayer bonding is of an ionic type. These materials have been classified as layer compound; however they do not meet the requirement for a layer structure, i.e. a van-der-Waals gap with weak interlayer bonding. Such layers can easily be disrupted mechanically leading to naturally cleavage planes of the material like in graphite. [38]

2.1.1 Chemical bonding

According to band structure calculations the layered crystal structure translates into a highly two dimensional electronic structure. The two dimensional nature of the ZrCuSiAs-type structure reflects chemical bonding pattern. Bonding interaction between atoms of different electro-negativities is responsible for the more or less pronounced ionic character of the ZrCuSiAs-type compound. Theoretical studies of this material shows a two dimensional electronic structure and that the conductivity takes place in FeAs layers while the REO layer provide the charge reservoir when doped with (Flourin) F ions. This is similar to that of cuprates materials. The superconductivity emerges when the mother compound is doped with electrons or holes and suppresses the magnetic order. The electronic and magnetic properties of ReOMPn changes with different transition metals M. For M= Mn, it is an antiferromagnetic insulator, for M= Fe, Ni it is a superconductor. It is ferromagnetic metal for M=Co. This indicates that no of 3d electrons plays a crucial role in magnetic and superconducting phases. The common feature in cuprates and Fe based superconductors is the superconductivity can be obtained by providing electrons or hole carriers to the 2D transport layers containing 3d transition metal elements such as FeAs layer. [39]. However, they differ distinctly from each other in that nine 3d electrons are involved for $Cu^{2+}O$, whereas six 3d electrons are involved for the FeAs bond with O. The presence of FeAs layer is common feature in all Fe pnictide superconductors, in which the Fe atoms form a regular square lattice just like the CuO_2 plane in cuprates. However the location of arsenic is not same for all Fe based compounds. Arsenic is not located in between the Fe ions but above and below the centre of Fe ions square. This arrangement of As ions plays an important role in the electronic and magnetic properties of the Fe pnictide. These properties also changes with different Rare earth materials, materials with incomplete f shell induces an additional magnetic interaction in the compound. [39]

2.1.2 Magnetic structure and phase diagram of $REO_{1-x}F_xFeAs$.

As I mentioned earlier the quaternary equiatomic REOFeAs compounds have rather simple structure, of alternating layers of Fe-As and Re-O layers where FeAs layers are thought to be responsible for superconductivity. The parent compound or undoped compound of these systems is not superconducting itself and exhibits both a structural and magnetic phase transition. This structural phase transition changes the crystal symmetry from tetragonal (space group P4/nmm) to orthorhombic (space group Cmma) and leads to an antiferromagnetical order with a spin structure, which is shown in Figure (2.3). This anomaly was shown to be caused by the spin density wave (SDW) instability. There is lot of experimental and theoretical work giving evidence that the anomaly caused by a SDW. As a function of temperature the resistivity of the undoped parent compound, which is not an insulator like the cuprates shows a drop around 150K, which shows the structural transition from tetragonal at high temperature to orthorhombic at low temperature. Furthermore the neutron diffraction studies showed that around 130K while still in monoclinic phase the compound develops a spin density wave.

The Figure (2.2) shows the temperature dependent resistivity and magnetization data, which shows the structural and magnetic transition. The different electronic states of iron in LaFeAsO and fluoride doped $LaFeAsO_{0.89}F_{0.11}$ have been studied in detail by ^{57}Fe Mossbauer spectroscopy [40]. The ^{57}Fe spectra proved spin ordering in LaFeAsO and its suppression upon doping. The isomer shifts of the arsenide oxides are close to the data observed for the phosphate. Below the antiferromagnetic ordering (T_0 = 138 K) LaFeAsO shows full magnetic hyperfine field splitting with a hyperfine field of 4.86 T [41]. The magnetic moment at the iron atoms was estimated to have values between 0.25–0.35μB/Fe atoms [40]. Previous experiments indicated that by Fluorine doping at the oxygen site the superconducting state can be realized in these compounds by suppressing the SDW order and be further enhanced by applying chemical pressure by using different rare earths with smaller ion radius or using high pressure synthesis method which leads to smaller lattice constants.

A theoretical calculation suggested that the enhancement of the density of states at the Fermi level either by carrier doping or pressure is playing a key role for the appearance of superconductivity. Spin density wave seems to be necessary for high transition temperature superconductors and this is the possible reason behind the low critical temperature in REFeOP, which does not show the SDW transition.

Spin density wave (SDW) and charge density wave (CDW) are the names for two similar low energy ordered states of solids. Both these states occur at low temperature in anisotropic, low dimensional materials. These both instabilities develop in the presence of Fermi surface nesting. Charge density wave (CDW) couples to the lattice while spin density wave (SDW) couples to the spin.

The cuprates HTSc families turned in superconducting by introducing dopants that create electrons and holes in the parent compound. The antiferromagnetic mother compound is a Mott insulator. Unlike in the case of cuprates the iron oxypnictides are metallic. This is due to direct orbital interaction between Fe atoms at 285 pm, while there is no direct d-orbital overlap observed in cuprates.[40] Figure (2.3) shows the comparison between the magnetic structure in the CuO_2 plane of the cuprates and the FeAs plane of Fe based superconductors. From the Figure (2.3a) we can see that if we remove the centre Fe ion from the structure of FeAs, the structure is similar to that of a CuO_2 plane. In FeAs based superconductors both the structural and magnetic transition can be suppressed by doping with fluorine or with the oxygen deficiency which is a similar situation compared to the copper oxide superconductors. [8].

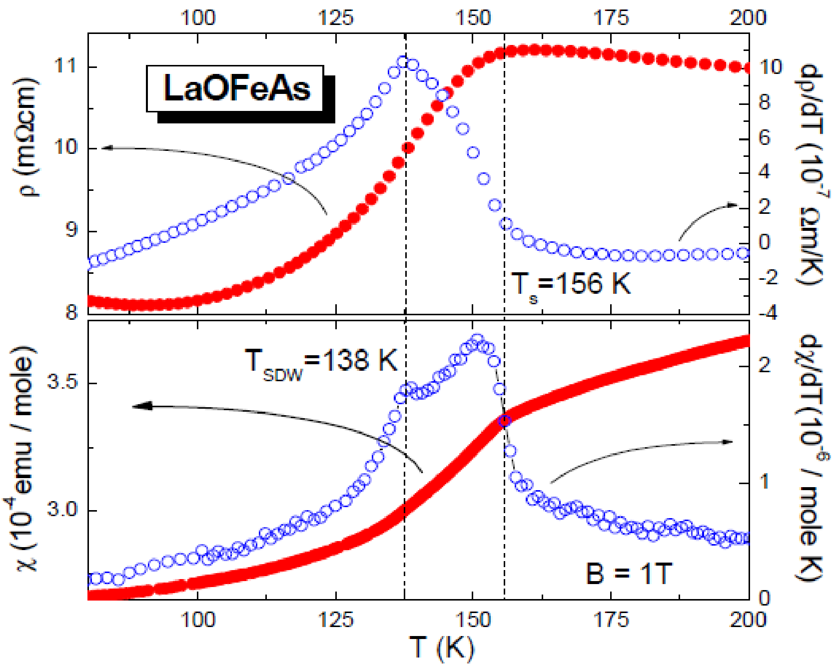

***Figure 2.2**: Temperature dependence of (top) the electrical resistivity and (bottom) the magnetization vs. Temperature. T_S and T_0 mark the structural phase transition at 156 K and the SDW-formation at 138 K respectively. [40]*

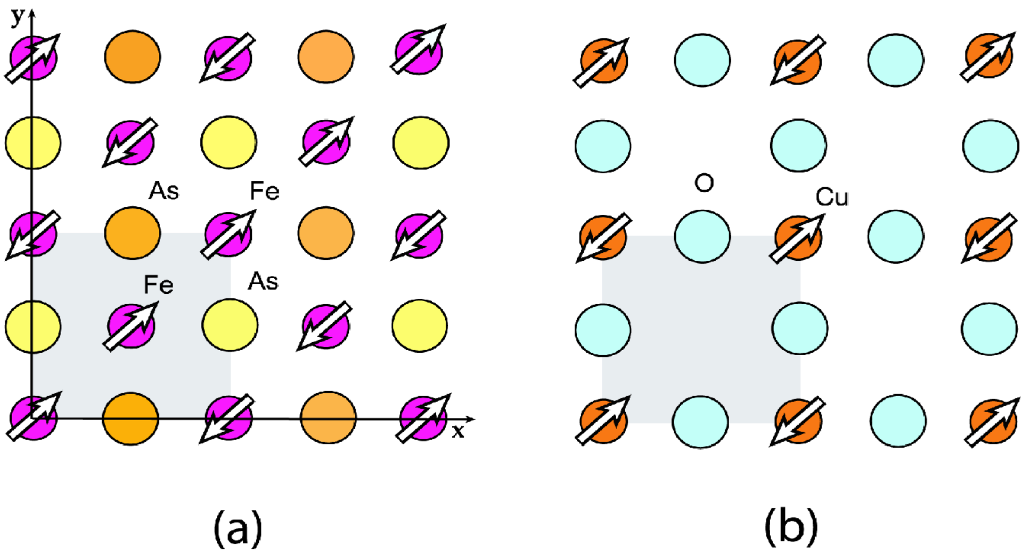

Figure 2.3 :(a) *The spin-density-wave (SDW) order as observed by the neutron diffraction. The Fe magnetic moments along the (1, 1) direction are aligned, while the two nearest neighboring Fe are antiferromagnetically aligned.* ***(b)*** *The familiar antiferromagnetic ordering of the cuprous oxides. The shaded square denotes the unit cell. The* CuO_2 *unit cell differs from the*Fe_2As_2 [31]

In REOFeAs compounds the superconductivity was discovered in $LaO_{1-x}F_xFeAs$ with 26 K with F^- doping. After that many group substituted La with other rare earths like, Sm, Nd, Ce, Pr, Eu according to the simple chemical formula $RE^{+3}O^{-2}Fe^{+2}As^{-3}$. With this substitution a transition temperature T_c of $SmO_{1-x}F_xFeAs$ up to 55K can be obtained. The other substituted rare earth ions have a smaller ion radius which is attributed to chemical pressure and responcible for the compression of lattice spacings results in a higher critical temprature Tc. The Figure (2.4(a)) shows the transition temperature dependence from the lattice parameter for different Rare earth compounds.[9-13]. The Figure (2.4(b)) shows temperature dependent resistivity of different rare earth oxypnictide superconductors.

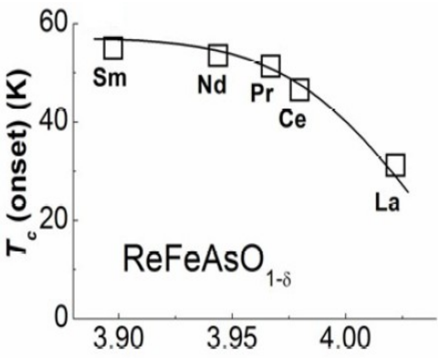

Figure 2.4(a): *transition temperature depending on lattice constant[8]*

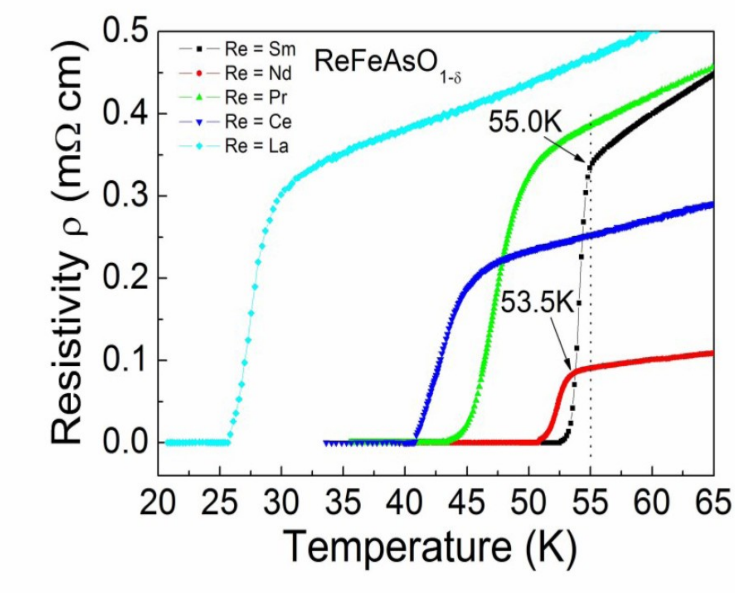

Figure 2.4(b): *Temperature dependent electrical resistivity for different rare earth ions.[8]*

Flourine doped

$CeO_{1-x}F_xFeAs$	41K
$PrO_{1-x}F_xFeAs$	52K
$NdO_{1-x}F_xFeAs$	51K
$SmO_{1-x}F_xFeAs$	43K
$GdO_{1-x}F_xFeAs$	36K

Doping by oxygen deficency

$LaO_{1-x}FeAs$	31K
$SmO_{1-x}FeAs$	55K
$CeO_{1-x}FeAs$	46K
$NdO_{1-x}FeAs$	53K
$PrO_{1-x}FeAs$	51K

Figure 2.4: *Table shows the different rare earth ion superconductors with Transition temperature.*

The table above represents the different rare earth matterials shows different transition temperature with flourine doping and with oxygen difficiency. The Origonal compound is $LaF_xO_{1-x}FeAs$ with Tc=26K. The μSR (muon spin resonace) transport measurement and mössbauer experiment is on the phase diagram of $REO_{1-x}F_xFeAs$ shows the first order like phase transition between antiferromagnetic and superconducting phases. These technique can detect the magnetic long range order but are not able to detect the structural distortion. On the other hand X-ray scattering detect structural transition but could not detect the AFM order so it is difficult to obtain the phase diagram with one of these two techniques alone . But neutron scattering is capable of detecting both the structural and magnetic transition (7). The Figure (2.5) shows the phase diagram of LaO$_{1-x}$ F$_x$FeAs with flourine doping of (x=0, 0.03, 0.05, and 0.08). According to this report LaO$_{1-x}$ F$_x$FeAs was found nonsuperconducting with doping x=0.03 , while with x=0.05 and x=0.08 it shows superconductivity at 8K and 26 K respectively.

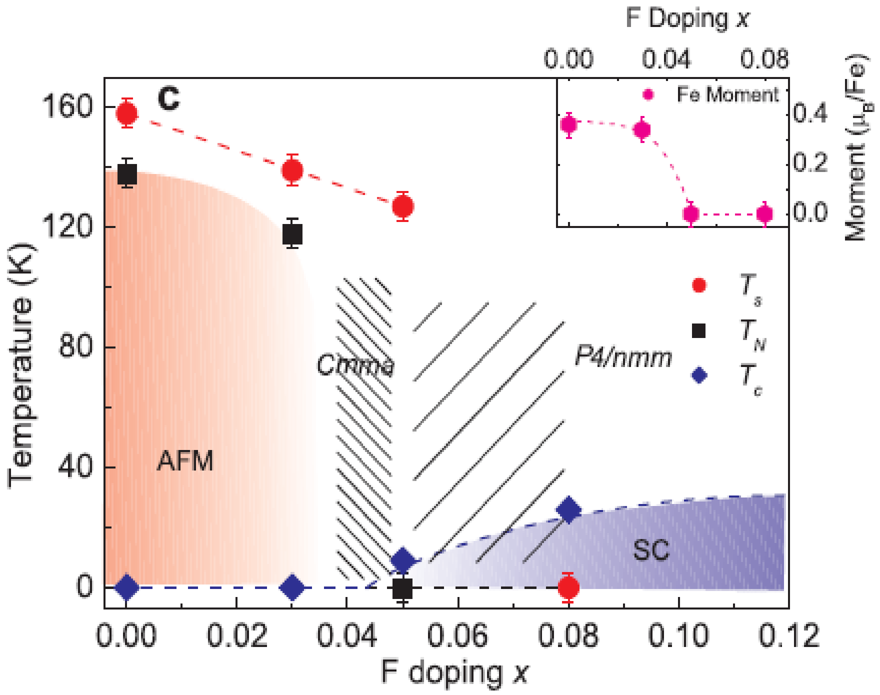

Figure 2.5: *Phase diagram determined from neutron measurements on LaFeAsO$_{1-x}$F$_x$ with x = 0, 0.03, 0.05, 0.08. The red circles indicate the onset temperature of the P4/nmm to Cmma phase transition. The black squares designate the Neel temperatures of Fe as determined from neutron measurements in [7] The inset shows the dependence of the magnetic moment from doping.*

2.1.3 Pressure effect

In the Fe_2As_2 layer, Fe and As ions form an $FeAs_4$ tetrahedron as shown in Figure (2.6) (b), because of the smaller ionic radius of Fe compared with As. At ambient pressure, the $FeAs_4$ tetrahedron is close to an ideal one with the As-Fe-As angle at (109.5) ° [32]. According to the As-Fe-As angle evolution with pressure, the distorted degree of the $FeAs_4$ tetrahedron increases with some pressure and then again decreases under higher pressure. When the pressure increases further, the Fe-As distance increases with pressure to reduce the dislocation of the $FeAs_4$ tetrahedron, in which the As-Fe-As angle drops and ions do not form a tetrahedron. Instead, RE ions have eight ligands including four (O, F) and four As ions, which form a distorted double tetraprism with a large RE-As distance which results in a lower transition temperature. The different coordination types from different ionic types contribute to the dissimilar compression behavior between the Fe_2As_2 and $La_2(O, F)_2$ layers. For LaOFeAs Tc=41 K was observed under external pressure of 4 GPa. [32]. While in CeOFeAs Tc lowers with external pressure. The Figure (2.6) shows the T_c can increase up to a certain limit, and after that Tc drops, due higher shrinkage of the lattice constant with application of pressure. Figure (2.6a) shows the effect of different applied pressures on the transition temperature of La111 compound.

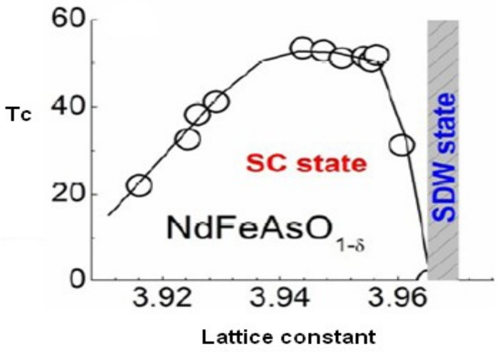

Figure 2.6: *Transition temperature dependent on lattice constant [*8]

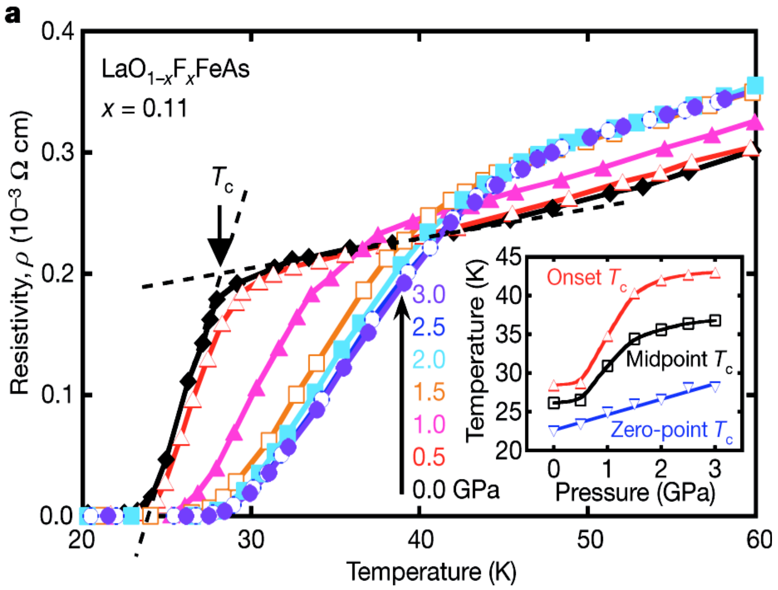

Figure .2.6 (a): *Temperature dependent resistivity of the La1111 with x=0.11 at different Pressures [32]*

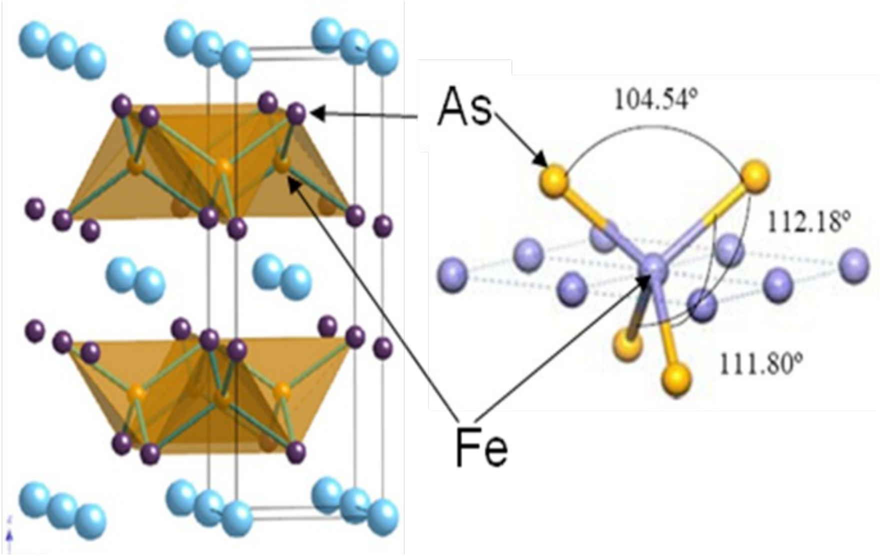

Figure 2.6(b): *crystal structure Of REOFeAs, in which FeAs ions forms the tetrahedral angle.*

2.2 Ternary Iron Arsenide ($A^{2+}Fe_2As_2$)

The tetragonal ZrCuSiAs structure type of REOFeAs compound is a layered structure. It is well known that the $ThCr_2Si_2$ structure type presents a very similar arrangement of the transition metal and pnictogen element. Thus after the discovery of REOFeAs it was natural for scientists to look for appropriate candidates within the huge amount of compounds crystallizing in this structure type. As I mentioned earlier, the REFeAsO compounds can be realized as a stack of alternating $(Fe_2As_2)^{2-}$ and $(RE_2O_2)^{2+}$ layers. Exchanging the $(RE_2O_2)^{2+}$ layer by a layer with a single large atom A (Alkali metal) leads to the $ThCr_2Si_2$ structure type. In order to keep the same electron counts as in the REFeAsO materials, A has to be a divalent atom. Therefore, appropriate candidates are $A^{2+}Fe_2As_2$ compounds, known as (122) family of iron arsenide based superconductors.

The family of FeAs based superconductors has been extended to double layered ternary iron arsenide AFe_2As_2 (A= Sr, Ba, Ca, Eu) (A: Alkali metals and Alkali -earth metals), so-called 122 systems. The ternary iron Arsenide AFe_2As_2 with tetragonal $ThCr_2Si_2$ type structure was first suggested by Rotter ref [15] it contains, identical edge sharing $FeAs_4$ tetrahedra. The crystal structure is similar to that of layered REOFeAs, only the REO is replaced by the Ba sheet in between FeAs layers. It does not contain oxygen which means that it not only breaks the monopoly of cuprates but also proved that the superconductivity of FeAs based superconductors are not associated with oxygen layers.

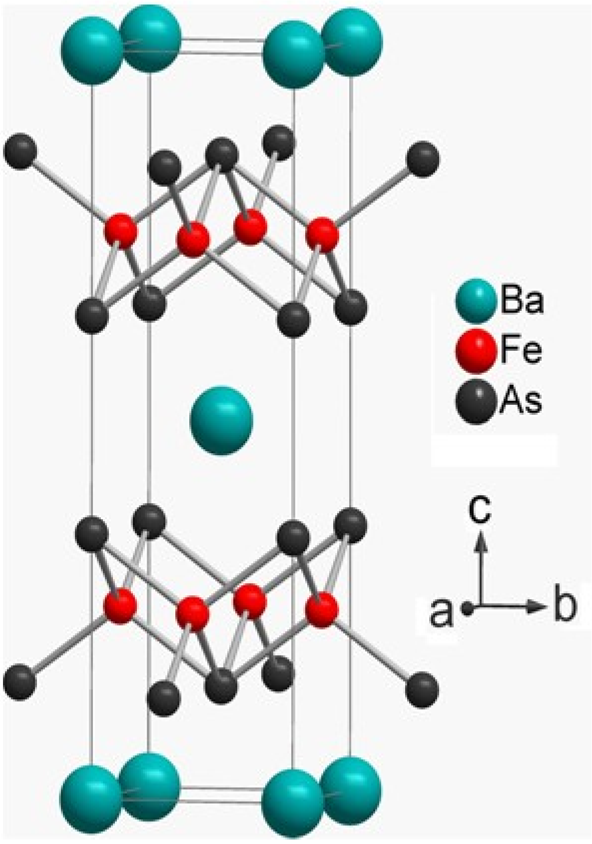

Fig2.7: *shows the crystal structure of $BaFe_2As_2$ [15]*

All the AFe_2As_2 compounds crystallize in the tetragonal $ThCr_2Si_2$ type structure. As in REOFeAs these compounds exhibits a similar SDW instability at 140K -205K for different alkali metals. It is therefore suggested that AFe_2As_2 could serve as a new parent compound for ternary iron arsenide superconductors. Shortly after that the superconductivity with transition temperature T_c =38K was found for hole doped $Ba_{1-x}K_xFe_2As_2$ by substituting K^+ for $Ba^{2+.}$ All parent compounds show a spin density wave (SDW) anomaly below a temperature of 140K and superconductivity associated with the suppression of the SDW. A suitable substitution on either the site A or the Fe site can suppress the magnetic ordering and then the system becomes superconducting for certain ranges of doping for example T_c= 38 K for $Ba_{1-x}K_xFe_2As_2$, Tc=32K for $Eu_{1-x}K_xFe_2As_2$ [15, 30] and Tc=20 for $SrFe_{2-x}$ CO_xAs_2, x=0.4 [29] T_c=24K $Ba(Fe\ Co)_2As_2$. Superconductivity can also be induced in undoped and under-doped compounds by applying pressure. [29]

The $BaFe_2As_2$ and REFeAsO series are almost identical in many properties, while the replacement of Ba by similar Sr or Eu^{3+} enhances the magnetic character of the FeAs layers. This is obvious from the ordering temperature which increases from T_0=150K to T_0=200K for

$EuFe_2As_2$ (T_0 is the phase transition temperature) and T_0= 205 K for $SrFe_2As_2$ that the phase transition temperature for Sr and Eu is almost the same is not surprising, since Sr^{2+} has almost the same ionic radius as Eu^{2+} and is often used as a non magnetic reference for Eu^{2+} compound. [17]

2.2.1 Crystal structure.

In this work we studied the properties of parent compound $BaFe_2As_2$ and doped $Ba_{1-x}K_xFe_2As_2$. The $BaFe_2As_2$ crystallizes in the tetragonal ThCr2Si2-type structure with two formula units per unit cell space group I4/mmm and crystal parameters a=0.39435 nm and c= 1.3118 nm. Like in oxypnictides the crystal structure is layered and formed by edge sharing $FeAs_{4/4}$ tetrahedrons with covalent bonding, interlaced by the layers of Ba2+ sheets perpendicular to [001] instead of (La-O) layers for LaOFeAs. The interlayer bonding is ionic, like oxypnictides. The quasi two dimensional characters of both compounds make them similar to the well studied class of superconducting copper oxides. The metal- metal bonding within the layers plays an important role in the properties of $ThCr_2Si_2$- type structure. Assuming the iron atoms are in the Fe^{2+}state ($3d^6$) the d shell is more than half filled and Fe-Fe anti bonding states should be at least partially occupied. The lowest lying bands are made by the overlap of the Fe-$3d_{x2-y2}$ orbital. Hence, the undoubtedly present Fe-Fe bonds (Fe-Fe= 0.2802 nm) in $BaFe_2As_2$ are slightly weakened, but more important less dispersed and mainly responsible for the magnetic properties. At 140 K $BaFe_2As_2$ undergoes a structural phase transition from tetragonal (I4/mmm) to orthorhombic (Fmmm) space group. It can be seen that for $BaFe_2As_2$ compound the Fe-As distance is smaller than LaOFeAs. So there is more considerable Fe-d-As-p hybridization, for $BaFe_2As_2$ system in comparison with LaOFeAs. It is stronger than the latter and as a result has a wider Fe-d bandwidth. The distance between the nearest Fe atoms within FeAs layers is also significantly smaller in AFe_2As_2 as compared with LaOFeAs system. After the structural transition to the orthorhombic structure the Fe-Fe distances are separated into two types of band width out of four bonds, the two pairs of bonds have a width of 0.2802 nm and the other two pairs have the width of 0.2877 nm. The angles between the Fe-As-Fe are also different than the oxypnictide systems. Such a difference in the adjacent Fe ions should lead to changes in their electronic structure.

As mentioned earlier similar to the oxypnictide systems the structural and magnetic transition also occurs in the AFe_2As_2. Superconductivity can be recovered by substituting the A ions by some impurity holes. The compound was doped by the chemical substitution of A^{2+} ions by potassium ions (K^{+}). While electrons are doped by the replacement of divalent iron atoms with trivalent cobalt (Co) or tetravalent nickel (Ni) ions T_c can be enhanced by applying pressure on doped or undoped compounds. The difference between the two systems regarding structural and magnetic transition are, in oxypnictide both the structural and magnetic transition occurs at different temperature .The magnetic transition occurs 10 to 20 K lower than the structural transition. While in AFe_2As_2 compounds it is found coupled and for same transition temperature. [25] The phase transition can see in Figure (2.6) phase diagram. The Figure (2.7) shows the lattice parameter dependence on the composition of the sample at room temperature. It is found that the changes are continuous and linear. The structural changes mainly affect the Fe-Fe bond length and the angle between the Fe and As.

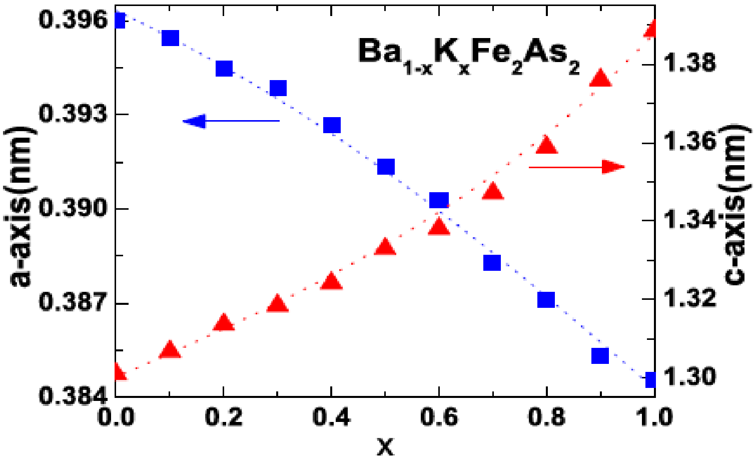

Figure 2.7:*Dependence of the lattice parameter with composition(25)*

The Figure (2.8) below shows the temperature dependent resistivity of the polycrystalline sample mesured by standared four probe with different doping . The Figure (2.9) shows the phase diagram of $Ba_{1-x}K_xFe_2As_2$. The phase transition was observed for the composition x=0 and x= 0.1 for $Ba_{1-x}K_xFe_2As_2$ at 150 K. We can see from the same Figure (2.8) that spin density wave (SDW) anamoly due to phase transition can be seen till the composition x=0.4 . The superconductivity arises at x=0.2 but still the anamoly can be seen. Spin density wave (SDW) is completely suppressed at x=0.4 and Tc increases till 37.5K. For the composition $Ba_{1-x}K_xFe_2As_2$ (x=1) the transition temperature is T_C=3.7K. In same paper they also describe the phase diagram based on neutron diffraction data. Almost the same phase diagram can be seen in ref(38). It is confirmed from the measurement of x ray structure, resistivity and Mössbauer effect . It can be see that the superconductivity and SDW coexist for $0.2 < x < 0.4$ [25]

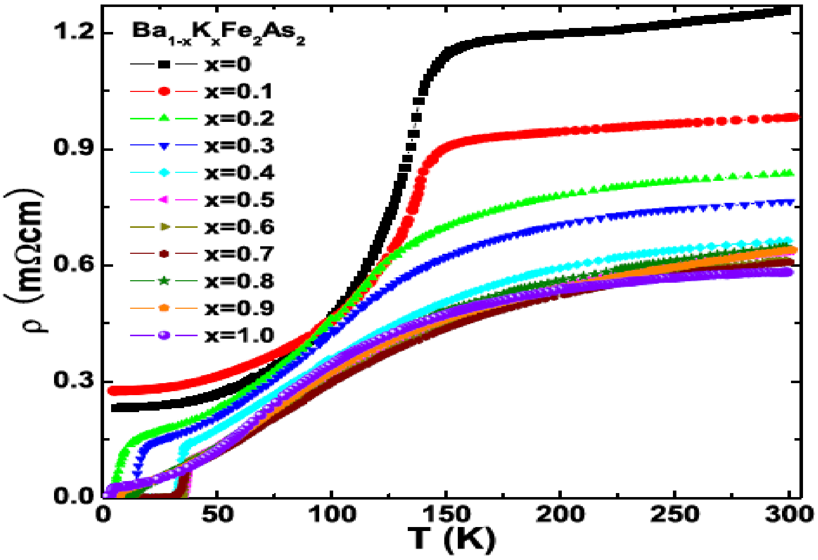

***Figure 2.8**: The resistivity depends on temperature. (25)*

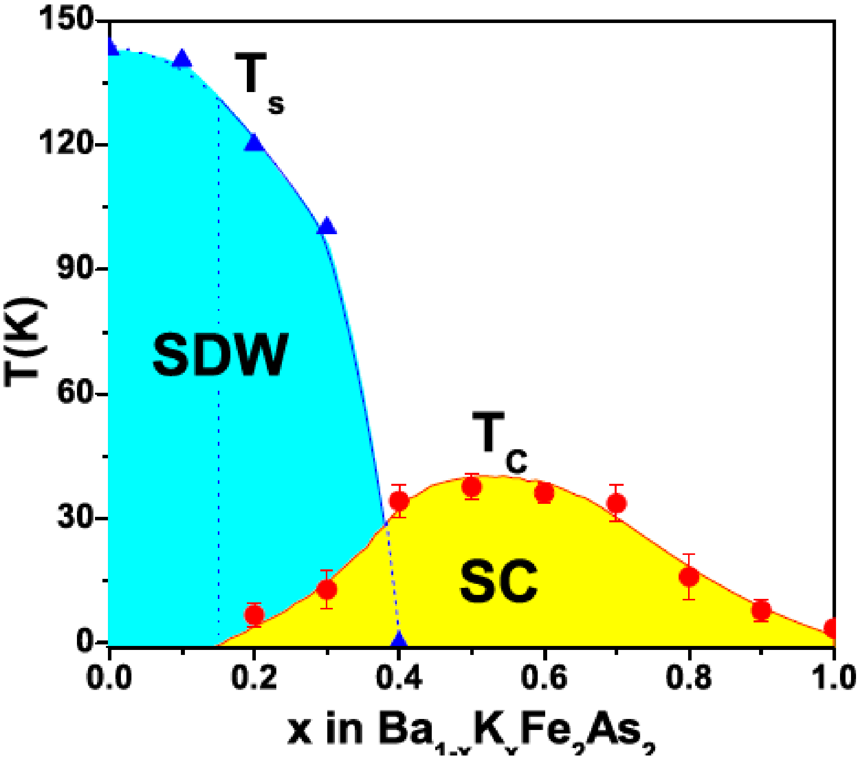

***Figure 2.9:** The composition-temperature phase-diagram, showing the structural, magnetic and superconducting transitions. The T_S denotes the temperature of the*

simultaneous structural and magnetic transition, and T_C the superconducting one. The spin-density-wave (SDW) and superconducting orders coexist at low temperature in $0.2 < x < 0.4$. [25]

It is interesting to note here that complete substitution with K^+ the ternary compound KFe_2As_2 is still superconducting with a transition temperature lower than T_c=4K. This makes this compound very useful to study the doping behavior. Though the transition temperature in ternary“122”compounds is still lower than the “1111” compounds, 122 is the extensively focused class of FeAs based superconductors.

2.2.2 Pressure effect on AFe_2As_2

Pure AFe_2As_2 (A= Ba, Sr, Eu) is not superconducting but shows a structural transition. Some reports stated that all the parent compounds which belong to the 122 family superconducts under pressure. [33]. First reports about pressure induced superconductivity in $CaFe_2As_2$ were recently discarded [43]. External pressure on this system creates a similar effect than doping. Application of pressure suppresses both the structural and the magnetic transitions and leads to the superconductivity in a similar way as charge substitution. The high pressure experiment indicates that superconductivity appears at approximately 2GPa to 6 GPa for $BaFe_2As_2$ and has a peak of Tc = 29 K near 4GPa[27,33], Sr Fe_2As_2 was first reported to superconducts at 2.5 GPa pressure with Tc =27 K [26,27, 33] and T_c decreases to below 20K with further increasing pressure up to 5.2 GPa

The main effect of pressure on the crystal structure of AFe_2As_2 is to shorten the Fe-Fe and Fe-As bond length and As- Fe-As bond angles. The angle changes slightly with a slight change in $FeAs_4$ tetrahedra, which is not equal to that of doped structure. In doped $A_{1-x}K_xFeAs$ the tetrahedral angle is about 109.5° which is ideal tetrahedral angle for superconductitivity, and transition temperature can reach value up to Tc=38K. While the parent compound under pressure the significant transition temperature can reach value up to 28K. It shows that superconductivity cannot improve only with external hydrostatic pressure on the parent compound but need uniaxial pressure to compress the Fe layer to make an ideal change in $FeAs_4$ tetrahedra to increase the transition temperature. Application of pressure has been widely used to explore the phase diagram of superconducting systems [26].

Superconductivity can also be achieved by substituting small amount of iron (Fe) by another d element such as Co (cobalt) and Ni (nickel). Doping on Fe site should directly affect the correlation in the Fe–As layers, where all the conduction activity takes place. This method might be useful to study the underlying physics of FeAs layer. Several groups reported superconductivity in Co doped compounds in both the classes $REO(Fe_{1-x}Co_x)As$1111 and $A(Fe_{2-x}Co_x)As_2$ 122. [28, 29]. The Pure Fe compounds $SrFe_2As_2$ undergoes a phase transition at T_0= 205K but Co substitution such as $SrFe_{2-x}Co_xAs_2$ leads to a decrease in T_0 followed by the superconductivity in the concentration range $0.2 < x < 0.4$. The transition temperature was observed at T_c=20K for x=0.4. For BaFe2−xCoxAs2As_2 x=0.12 the transition temperature is observed at Tc=22K.[29,48]

Chapter 3

3. Generic properties based on theoretical & experimental investigation

Comparing the 1111 and 122 ferropnictide compounds with each other, it becomes obvious that they have certain aspects in common. For example, their carriers are sharply localized in the planes perpendicular to the c-direction, making the material extremely anisotropic which means that they are, almost 2-dimensional with interlayer coupling in both the normal and the superconducting state. This is the case for all high-temperature superconductors. In the case of FeAs based superconductors, the electronic activities take place in the square FeAs planes. The interlayer planes are purely ionic; their sole purpose is to act as dopant reservoirs.

3.1 Electronic states

Superconductivity is a manifestation of quantum mechanics on a macroscopic scale. It is important to find whether the superconductivity in the new class of Fe based superconductors is conventional or unconventional like in the cuprates or have an entirely new mechanism. In conventional superconductors, it has been well established that electrons form so called cooper pairs to give rise to the superconductivity. The pair binding manifests itself as an energy gap in many spectroscopic measurements, the energy gap known as superconducting gap, appears at the transition temperature T_c where the resistance also vanishes. For high temperature superconductors this is more complicated since over the wide region of compositions and temperatures this energy gap exists quite well above the transition temperature and there is no relation between transition temperature and this energy gap. This is why this gap is called pseudo gap. The origin of pseudogap and the relation with the superconducting gap is believed to be the key to understand the mechanism of high temperature superconductivity.

All the conventional superconductors are well understood within the BCS theory as phonon mediated pairing of electrons and condensation of the resulting bosonic gas. All superconductors that can be understood within this theory have a transition temperature less than 40K. Preliminary experimental results such as specific heat (33), NMR spectroscopy (35) and high field resistivity measurement suggest the existence of unconventional superconductivity in these Fe based superconductors.

It is pointed out in some papers (18, 19) that there is an essential similarity of electronic states near the Fermi level in 122 and 1111 family. Both families have been studied in many details by DFT (density functional theory) calculation. DFT is the quantum mechanical theory used in physics to investigate the electronic structure of many body systems principally the ground state. DFT in principal gives a good description of ground state properties. Practical application s of DFT is based on approximations for so called exchange co-relation potential. The exchange describes the effects of the Pauli principle and the coulomb potential beyond pure electrostatic interactions of the electrons. A common local density approximation (LDA) which locally substitutes the exchange co-relation energy density of an inhomogeneous system by that of an electron gas evaluated at the local density. (36)

LDA calculations predict that pure Fe pnictide of both 1111 and 122 classes possess a ferromagnetic instability due to very high density of states. In the Fe-As layers, the Fe atoms are bonded with four As atoms in tetrahedron for both families. The Fermi surface and band structure of these compound are similar. The Fermi surface calculations for $BaFe_2As_2$ and LaOFeAs are shown in the Figure (3.2) (36). The band around the Fermi level for both compounds is mainly formed by Fe-d orbitals. We can see from Figure (3.1), the Fe 3d orbitals are the main contributors to the density of states together with the very small contribution from As-p orbital. The states at the Fermi levels have contributions from spin d_{yz} and d_{x2-y2} orbitals. In this sense we can say that all phenomena related to superconductivity in these compounds take place in the square lattice of Fe within the FeAs layer.

From the Figure (3.1) we can see that the values of the density of states at the Fermi level are similar for both the types 1111 and 122, but in the case of $BaFe_2As_2$ because of shorter Fe-As bonds and stronger Fe-d-As-p hybridization the Fe-d band is shorter.

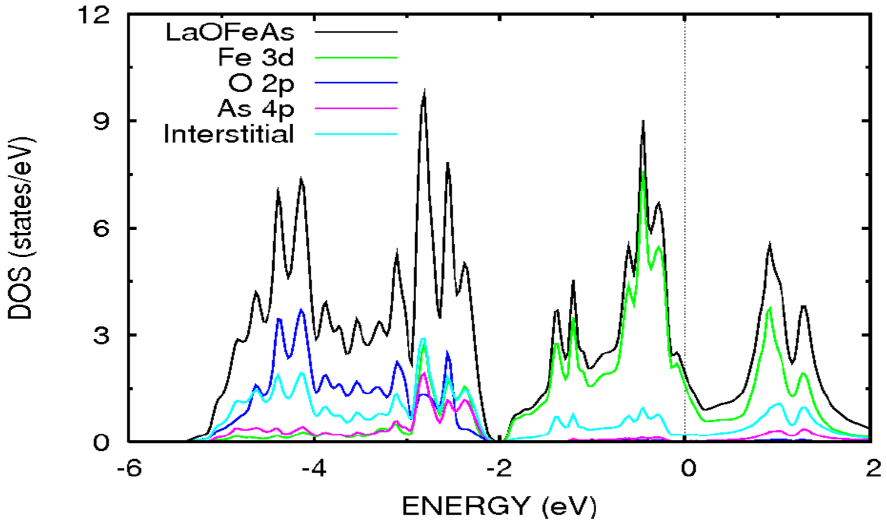

(a)

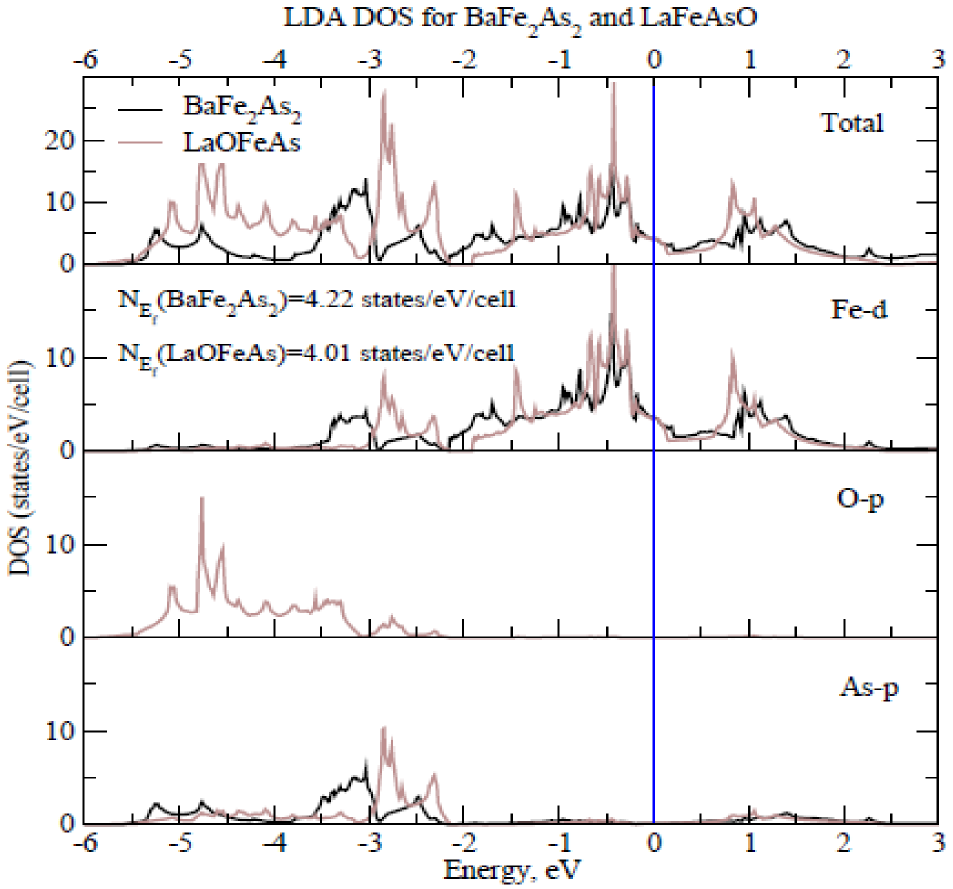

(b)

Figure 3.1: ***(a)*** *LDA DOS (44) for LaOFeAs The total and partial LDA DOS for BaFe2As2 (black lines) and LaOFeAs compound (36)*

The available electronic structure calculations of Fe oxypnictide convey the key information that all five Fe 3d are located at the Fermi level this is different than cuprates. There are five sections of the Fermi surface two concentric hole pockets Γ1 and Γ2 centered at Γ [k= (0, 0)] point which are hole type Fermi surface and mostly come from d_{yz} and d_{zx} states of Fe. In addition the electron elliptical pocket centered at M [k= (π,π)], mostly come from the d_{xy} and $d_{yz/zx}$ states of Fe. The shape of ellipse comes from the hybridization between d_{xy} and d_{yz}. The stronger the hybridization, the more the distortion of the ellipse. These ellipses have the same size but turned are in to 90 ° to each other. There is one 3d hole band with spherical Fermi Surface around z point the last one vanishes upon doping, which is the smallest one and usually neglected in the analysis of superconducting pairing because of its smaller space volume it is believed that its contribution to the electronic properties is comparatively smaller (36)

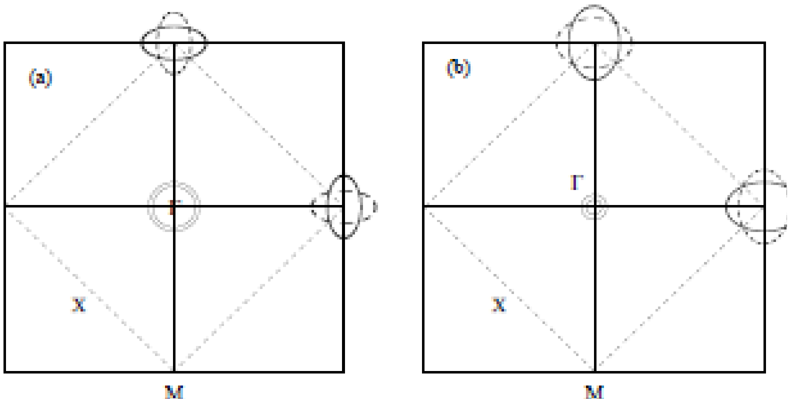

Fig3.2: *schematic plots for Fermi surfaces of LaOFeAs, Figure (a) is for pure LaOFeAs and Figure (b) is for LaOFeAs with 20 % F-doping. The large square represented the brillouin zone for one Fe cell, while the small diamond is the brillouin zone for two Fe cell. Figure (b) shows* the electron for doped distorted ellipses as compare to the Figure (a).(37)

It is clear that this kind of a band structure shown in the Figure (3.1) leads to similar Fermi surfaces of 1111 and 122 compounds, as it is shown in the Figure (3.3). As mentioned earlier there are three hole like cylinders at the center of Brillouin zone and two electron like at the corners. The almost cylindrical form of the Fermi surface reflects the quasi two dimensional nature of the electronic spectrum in these new superconductors. The brillouin zones for the two types of compounds are similar with a slight difference due to their lattice parameters.

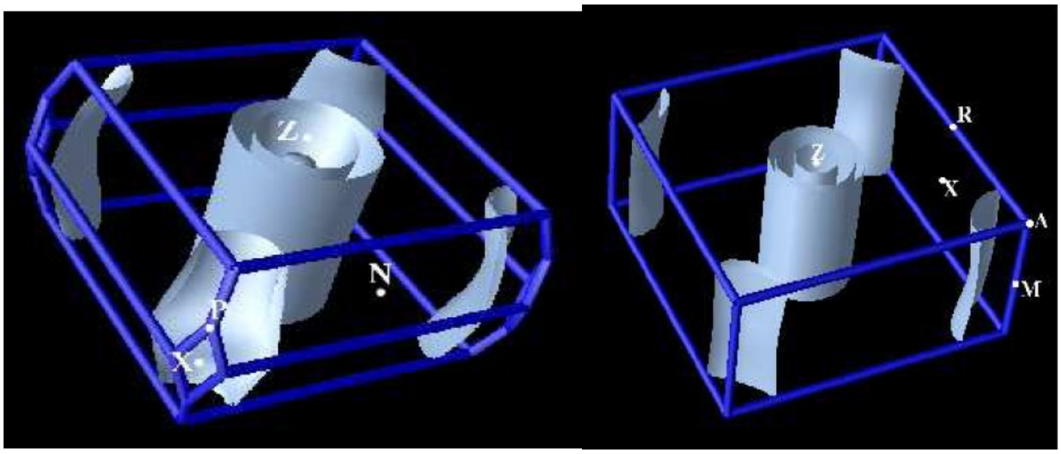

Figure3.4: The Fermi surfaces for $BaFe_2As_2$ (left side) and for LaOFeAs (right side) , (36)

The density of states (DOS) for holes and electrons is comparable for undoped material, but with doping either holes or electrons become dominant. The undoped compounds shows the structural (tetragonal to orthorhombic) phase transition and magnetic transition is attributed to spin density wave (SDW) formation due to the nesting of the Fermi surfaces. Doping suppresses this long range magnetic order, which is believed to be prerequisite for superconductivity in Fe based superconductors. Supercondtivity arises due to destruction of magnetic coupling between the layers.

In the superconducting state, the electrons pair and condense into a low energy state leading to the formation of a gap at the Fermi energy E_f. It is this gap that protects the superconducting condensate. A perfectly symmetrical gap which is equally spaced above and below the Fermi level is a strong indication that electrons are paired up. That superconducting gap exists at and below the transition temperature. One of the most prominent differences when comparing high-temperature superconductivity with metallic superconductors is that the symmetry of the superconducting order parameter is *d*-wave like in cuprates. In BCS theory the order parameter coincides with half of the total energy gap $2\Delta\mathbf{k}$ in the electronic density of states. Hence the quasi particle dispersion exhibits gapless nodes at the Fermi surface along the diagonals of the Brillouin zone. Based on the general space group of the material, and together with the detailed pairing interaction between the two electrons, the superconducting gap should have a specific symmetry for an individual superconductor

A number of different scenarios have been proposed to explain the mechanism of the superconductivity in Fe based systems, with predictions about the symmetry of the order parameter ranging from isotropic and anisotropic s-wave to d-wave and p-wave symmetry. Angle Resolved Photo Emission Spectroscopy is one of the most direct methods of studying the electronic structure of the surface of solid .The angle resolved photoemission spectroscopy (ARPES) technique is the reliable technique to measure not only the Fermi surface but also the superconducting gap There are already a number of papers, where the electronic spectrum and Fermi surfaces in these new superconductors were studied using the angle resolved photoemission spectroscopy (ARPES) technique. But comparatively less amount of work has been done on 1111 type due to lack of nice single crystals in this type of superconductors. The different gaps have been observed in several compound classes by a variety of experiments. In ref. (21) ARPES measurement has been done on the $NdO_{0.9}F_{0.1}FeAs$ system. The momentum dependence of the superconducting gap in the hole pocket around Γ (0, 0, 0) and cylindrical electron pocket at each corner of the Brillouin zone (M) was estimated from this and found to measurement have a magnitude of 20 meV, which would correspond to $2\Delta\mathbf{k}/T_c \approx 8$. This result is quite similar to the values reported by local density approximation LDA calculations.

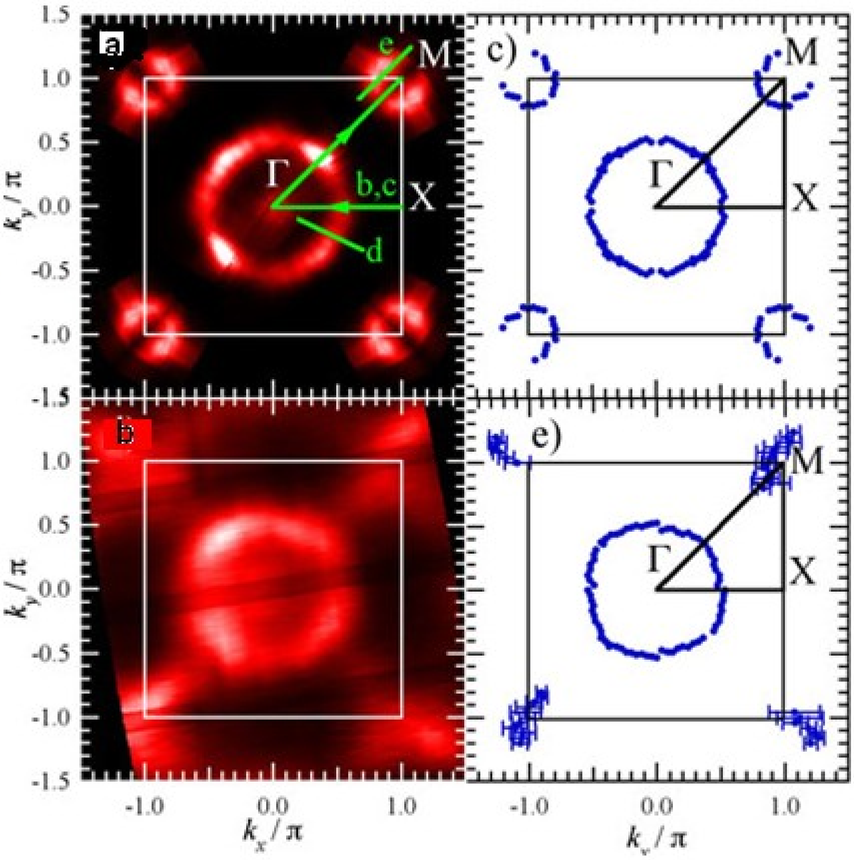

Figure 3.5: *ARPES intensity map as a function of k_x and k_y momentum, integrated within 20 meV of the Fermi energy. Bright areas mark the location of the Fermi surface.(21) where a and b are the intensity map and c and e are the Fermi surfaces at photon energy 22ev and 77 ev respectively.*

The another ref (22) measured ARPES on single crystals of the $Ba_{0.6}K_{0.4}Fe_2As_2$ superconductor with Tc =35 K and found the multiple nodeless superconducting gap (22). They observed multiple Fermi surface sheets in this compound. Two hole-like Fermi surface sheets around the Γ point exhibit different superconducting gaps. An inner Fermi surface showed large gap of Δ=12meV, which is slightly momentum dependent while the outer Fermi surface shows the smaller gap of Δ=7 to 8 meV, which is nearly isotropic. Similar results were found in ref (23). The ARPES measurement on $Ba_{0.6}K_{0.4}Fe_2As_2$, T_c=37 shows two superconducting gaps. A large one at Δ=12meV on small hole like cylinder around Γ and also hole like cylinders around point M and small one Δ=6meV on big hole like cylinder around Γ point . Both gaps are nearly isotropic on specific Fermi surface sheets. Accordingly the 2Δ/Tc ratio is different on different Fermi surfaces. These results of nodeless gaps are corresponding to the generalized S wave pairing (23). The following Figure (3.6) shows the three dimensional picture of the superconducting gap of size Δ in $Ba_{0.6}K_{0.4}Fe_2As_2$. The inset shows the temperature dependence of the gap on different Fermi surfaces.

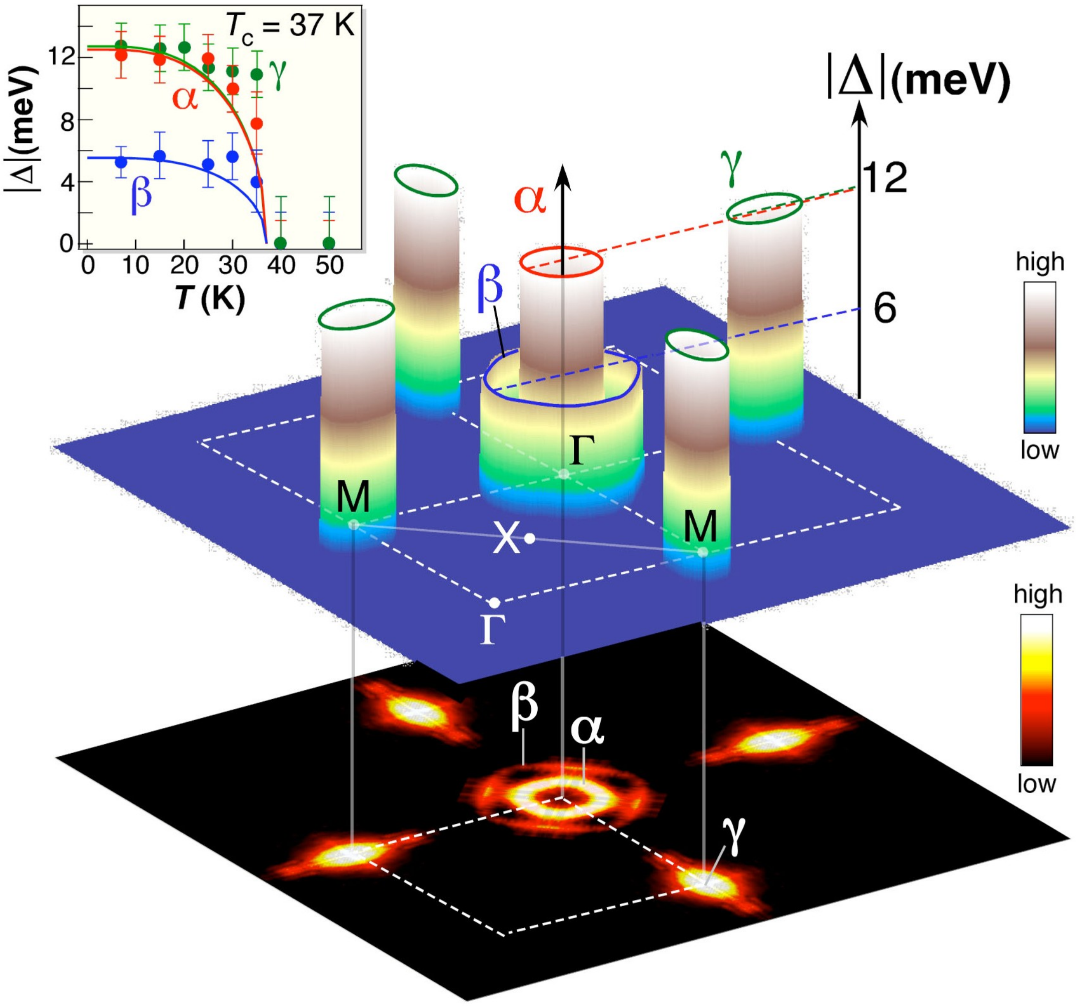

Figure 3.6: *Three dimensional picture of the superconducting gap in* $Ba_{0.6}K_{0.4}Fe_2As_2$ *(measured by ARPES at 15K) The inset shows the temperature dependence of superconducting gaps on different Fermi surfaces represented by different colors (23).*

The above ARPES measurements have been performed for both 1111 and 122 materials. They demonstrated the existence of a well defined Fermi surface that consists of hole and electron pockets which is in agreement with the predictions of electronic structure calculation. [45]

Chapter 4

4. Experimental Techniques

In this Chapter, the experimental techniques used in this work are described. In this work, the crystals were identified by X ray powder diffraction (XRD) using Cu Kα radiation .The chemical composition was determined by energy dispersive X-ray analysis (EDX). The crystal morphology was studied by a scanning electron microscopy (SEM). The temperature dependence of the electric resistivity for the pure and doped polycrystal and single crystals was investigated using a standard four point technique measured from 4 to 300 K. The ac-magnetic susceptibility measurements were performed by a superconducting quantum interference device magnetometer (SQUID) in different fields.

4.1 Structural Analysis

About 95% of all solid materials can be described as crystalline. When X-rays interact with a crystalline substance, X-ray diffraction results from an electromagnetic wave (the X-ray) impinging on a regular array of scattering sites (the repeating arrangement of atoms within the crystal). One gets a diffraction pattern. A X ray diffraction pattern of the pure substance is therefore, like a fingerprint of the substance. The powder diffraction method is thus ideally suited for characterization and identification of polycrystalline phases. A X-ray diffractrometer consist of three elements: X-Ray tube, a sample holder, and X-ray detector. X-rays are generated in a cathode ray tube by heating a filament to produce electrons accelerating the electrons towards a target by applying a voltage, and bombarding the target material with electrons. When electrons have sufficient energy to dislodge inner shell electrons of the target material, characteristic X-rays spectra and Brehmsstrahlung are produced. Copper is the most common target material for single-crystal diffraction, with CuK$_\alpha$ radiation 0.5418Å. These X-rays are collimated and directed onto the sample. As the sample and detector are rotated, the intensity of the reflected X-rays is recorded. The interaction of the incident rays with the sample produces constructive interference (and a diffracted ray) when the conditions satisfy Bragg's Law ($n\lambda = 2d \sin\theta$). This law relates the wavelength of electromagnetic radiation to the diffraction angle and the lattice spacing in a crystalline sample. These diffracted X-rays are then detected, processed and counted. By scanning the sample through a range of 2θangles, all possible diffraction directions of the lattice should be attained due to the random orientation of the powdered material.

Figure (4.1) shows that the incoming beam coming from upper left side causes each scattering site to re-radiate a small portion of its energy as a spherical wave. If atoms are arranged symmetrically with a separation d, these spherical waves will be add constructively only in directions where their path-length difference $2d \sin\theta$ equals an integer multiple of the wavelength λ. In that case, a part of the incoming beam is deflected by an angle 2θ, producing a reflection spot in the diffraction pattern.

The structure and phase purity of the as grown crystals were identified by XRD. The XRD diffraction patterns were obtained using ground powders of as-grown single crystals of the parent compound of $BaFe_2As_2$, and $Ba_{1-x}K_xFe_2As_2$ and polycrystalline sample of $SmO_{1-x}F_xFeAs$. The lattice parameters are derived from the powder XRD data. The results are discussed in the next section.

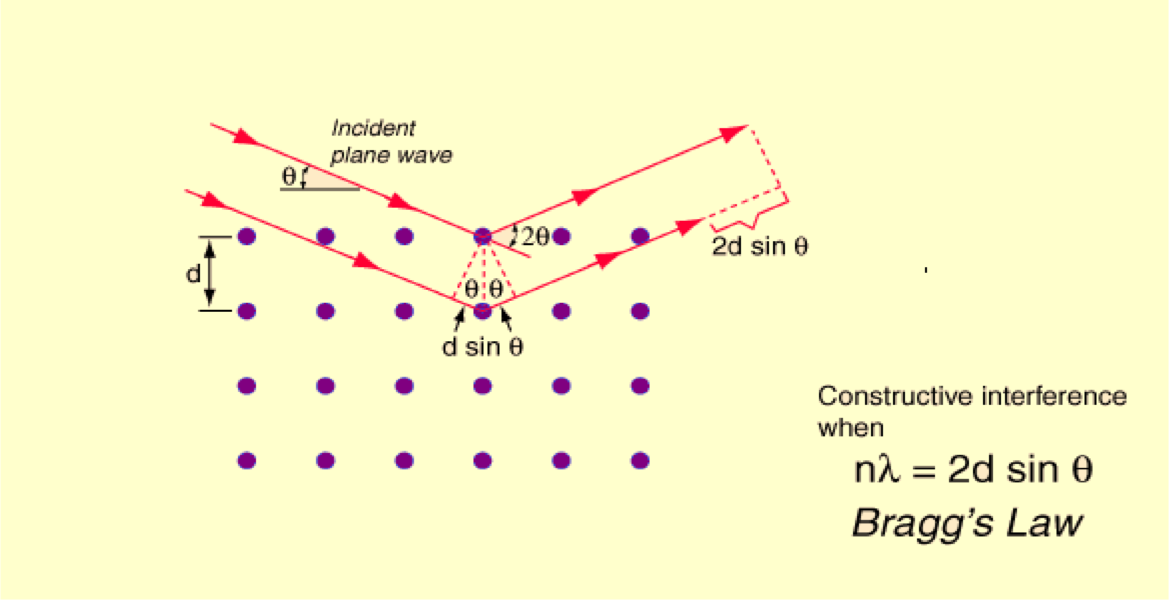

Fig4.1: Bragg's diffraction

4.2 EDX (Energy Dispersive X-ray analysis).

EDX is a technique used for identifying the elemental composition or chemical characterization of the specimen, or an area of interest on the sample. It relies on the investigation of a sample through interactions between electromagnetic radiation and matter. The EDX analysis system works as an integrated feature of a scanning electron microscope (SEM), and cannot operate on its own without the other. Scanning electron microscopes are equipped with a cathode and magnetic lenses to create and focus a beam of electrons. The fundamental principle that each element has a unique atomic structure allowing x-rays that are characteristic of an element's atomic structure to be identified uniquely from each other.

During EDX Analysis, the specimen is bombarded with an electron beam inside the scanning electron microscope. The bombarding electrons collide with the specimen atoms' own electrons, knocking some of them off in the process. A position vacated by an ejected inner shell electron is eventually occupied by a higher-energy electron from an outer shell. To be able to do so, however, the transferring outer electron must give up some of its energy by emitting an X-ray. The amount of energy released by the transferring electron depends on which shell it is transferring from, as well as which shell it is transferring to. Furthermore, the atom of every element releases X-rays with characteristic energy during the transferring process. Thus, by measuring the characteristic energy present of the X-rays being released by a specimen during electron beam bombardment, the identity of the atom from which the X-ray was emitted can be identified.

The output of an EDX analysis is an EDX spectrum .The EDX spectrum is just a plot of how frequently an X-ray is received for each energy level. An EDX spectrum normally displays peaks corresponding to the energy levels for which the most X-rays had been received. Each of these peaks are unique to an atom, and therefore corresponds to a single element. The higher the peak in a spectrum, the more concentrated the element is in the specimen.

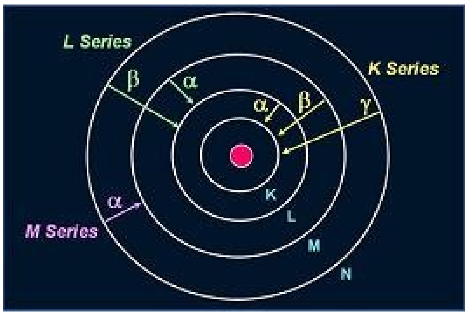

Figure 4.2: Different Energy shell

Elements in an EDX spectrum are identified based on the energy characteristic of the X-rays emitted by their electrons as these electrons transfer from a higher-energy shell to a lower-energy one. An EDX spectrum plot not only identifies the element corresponding to each of its peaks, but also the type of X-ray to which it corresponds as well. For example, a peak corresponding to the amount of energy possessed by X-rays emitted by an electron in the L-shell going down to the K-shell is identified as a K-Alpha peak. The peak corresponding to X-rays emitted by M-shell electrons going to the K-shell is identified as a K-Beta peak. See above Figure (4.2)

4.3 SEM (scanning electron microscopy)

The scanning electron microscopy is used for inspecting topographies of specimens at very high magnifications. During SEM inspection, a beam of electrons is focused on a spot volume of the specimen, resulting in the transfer of energy to the spot. These bombarding electrons, also referred to as primary electrons, dislodge electrons from the specimen itself. The dislodged electrons, also known as secondary electrons, are attracted and collected by a positively biased grid or detector, and then translated into a signal.

To produce the SEM image, the electron beam is swept across the area being inspected, producing many such signals. These signals are then amplified, analyzed, and translated into images of the topography being inspected. Finally, the image is shown monitor.

In this work we use this technique to study the topography of single crystals of the 122 system.

4.4 SQUID

SQUID the abbreviation stands for superconducting quantum interface device. I used this technique to measure the magnetization of a sample as a function of parameter such as the external magnetic field H or the temperature T. The SQUID magnetometer MPMSXL-7 manufactured by Quantum Design provides a magnetic field of $-7T \leq \mu 0H \leq +7T$ at a temperature range of $1.8K \leq T \leq 400K$ in the sample space . The schematic diagram of SQUID can be seen in the Figure (4.3).

Second order gradiometer suppresses the pickup of all static magnetic fields and all signals homogeneous over the gradiometer length including the sample holder. The current induced by the movement of magnetic sample inside the gradiometer pick up coils are flux coupled in to the SQUID loop. The SQUID is highly sensitive magnetometer of resolution 10^{-8} emu ($=10^{11}$ Am^2) in the RSO mode (rapid sample oscillations).The high sensitivity of the SQUID devices is associated with measuring changes in magnetic field associated with one flux quantum

$$\phi_0 = \frac{2\pi\hbar}{2e} = 2.0678 \times 10^{-5} tesla.m^2$$

The MPMSXL-7 SQUID magnetometer can only measure the vertical component of magnetization which is parallel to gradiometer axis and hence parallel to the external magnetic field.

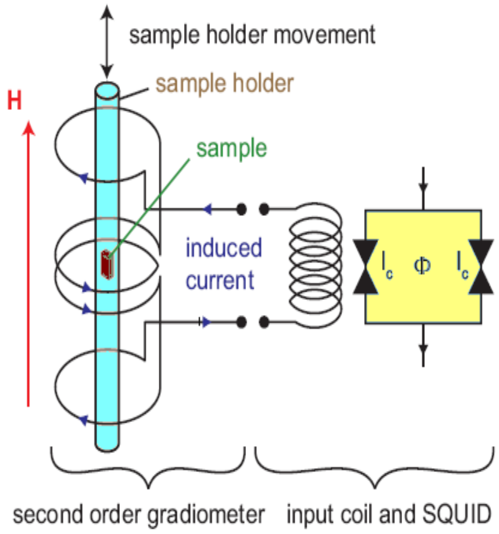

Figure 4.3: *schematic diagram for SQUID magnetometer[42]*

4.5 Magneto transport Measurement

Magnetotransport measurement has been performed using a cryostat equipped with a 17Tesla magnet system. The quantities to be measured are resistivity and the hall coefficient. These quantities are measured within a temperature range 1.5 K to 300 K in magnetic fields up to 14T. A sample temperature up to 390K can be achieved using this system. The magnetic field is generated using a single superconducting coil held at liquid He temperatures in the ^{4}He space of the magnet cryostat. A variety of sample holders can be mounted allowing for e.g. sample rotation during the measurement. All measurements are fully computer controlled by the use of the LabView software tool allowing for remote access. A cryostat with variable temperature inserts (VTI) and superconducting magnet system from Oxford instruments was used for the measurements. The sample has been mounted on a dipstick and then the dipstick was put into the cryostat. The temperature can be controlled using (ITC) intelligent temperature controllers from Oxford instruments. It can measure and control the temperature with precision of a few mK by using a lakeshore 340 temperature controller by measuring the resistance of a calibrated cernox resistor.

A VTI consist of long tube fixed in to tank. The space between the two is filled with helium gas or vacuum so that the sample space is thermally isolated from the environment. When the VTI is submerged in to helium bath the sample space is continuously pumped. The temperature controller reads the temperature dependent 60Ω resistance of the cernox resistor next to the sample and regulates the heater power of the sample heater. Both heater and censor are mounted very close to the sample position, so it can give the accurate temperature measurement. Cooling is realized by a bath of liquid ^{4}He surrounding the superconducting coil completely. To apply a stable magnetic field one can run the magnet, into persistent mode, to energize the magnet. The temperature of the switch increases above the Tc by a heater source. After switching off the heater the superconducting coil is disconnected from current source and field, which corresponds to the applied current, is frozen. Figure (4.3) shows the schematic diagram of cryostat.

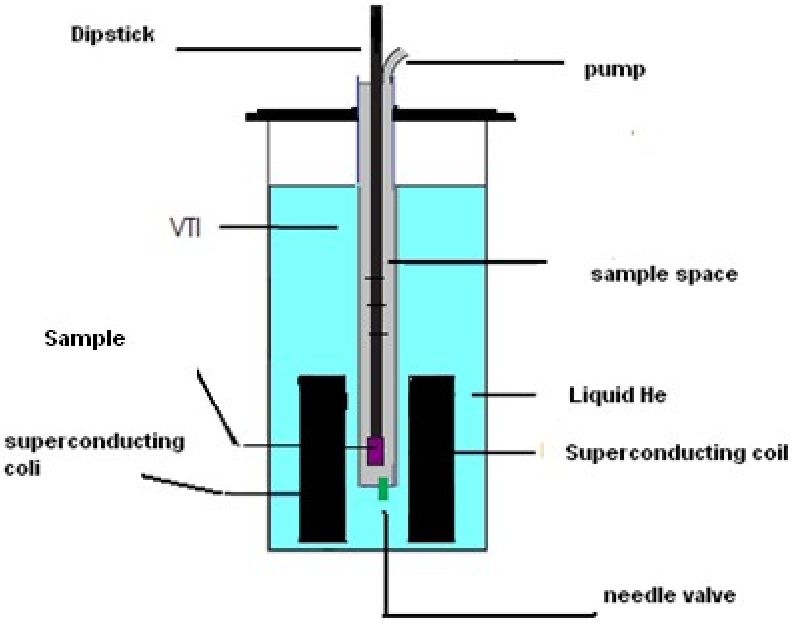

Figure 4.3: *schematic diagram of cryostat.*

4.5.1. Measurement setup

For the voltage measurement, in this work we used a DC nanovoltmeters or a Lock in technique depending on the amplitude of signal. The simplest way to measure the resistivity is the standard four point method. The DC current was applied on pin (1, 2). The voltage was measured with a multimeter on the other two pin (3, 4). Typical current values range from 1 – 10mA.

For the DC current source a keithley 2400 sourcemeter and for the voltage measurement the low noise keithley 2010 voltmeter were used they were controlled remotely using Lab view program. The highest resolution of both multimeter types is 10nv and 1nv respectively.

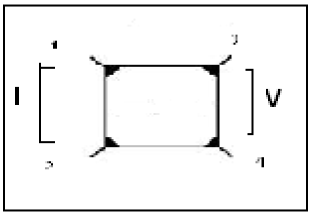

Figure 4.4:*contacts at the corner of single crystal.*

4.5.2 Sample holder preparation

In this work we used two types of sample 1). Polycrystalline sample of $SmO1_{-x}F_{x}FeAs$ from REOFeAs (1111) family and 2) single crystal of $Ba_{1-x}K_{X}Fe_2As_2$ (122) family. For the polycrystalline sample we made powder of that sample using mortar and pestle. And then pressed the powder in to bar using a anvil press.

The sample was contacted with 20 µm gold wires and silver paste (Dupont 4929). The contacts were not so stable and got off from the sample within one temperature cycle from 300K to 1.7K. To solve this problem, we did gold sputtering on the single crystal surface. For this purpose the crystals were masked with scotch tape leaving free the four corners of the sample and then did sputtering on the masked sample which was about 100nm thick. After approximately 3 hours, we removed that tape from the sample and cleaned the sample with acetone. Thereafter, the contacts were applied with gold wire and silver paint on the sputtered gold film at the corners of the sample. The contact resistances, achieved by simply drying under ambient condition for at least 12 hours are in the range of few ohms. These contacts were low ohmic contacts, which is crucial to get a low noise signal. The sample holder with polycrystalline sample is shown in Figure (4.5).

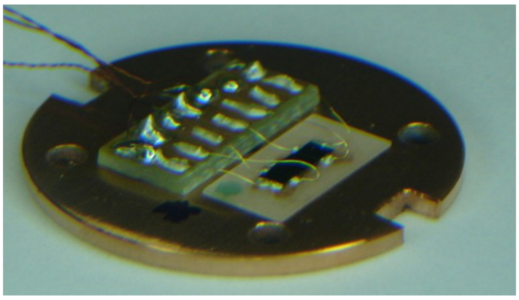

Figure 4.5: sample holder with contacted sample

4.5.3 Gold Sputtering

To set the stable contacts on top of single crystals, we used the gold sputtering method . For very fine sputter coated films, we required high vacuum sputtering. First the residual gas component is virtually eliminated from the vacuum chamber by a high vacuum pump. The working pressure required for sputtering is approximately 10^{-2} mbar it has been established with entering the argon gas in the chamber. We wanted the thin sputtering only on the corners of the single crystal sample. For this purpose, we covered the sample with thin strips of scotch tape leaving free the corners of the sample and then did the sputtering on that sample.

To start the sputtering process high voltage was applied to the target (cathode). This produces a high voltage electric field between the target and the specimen table (anode). The free electrons in this field are forced into a spiral path by a magnet system, where they collide with the argon atoms in the field. Each collision knocks out an electron of the outer shell of the argon atom .The positively charged argon ions are accelerated to the cathode (target) where they impinge, knocking off metal atoms as they hit. Collisions also occur between the metal atoms thus released and the other gas molecules in the vacuum chamber. This causes the metal atoms to scatter widely, forming a diffuse cloud. The metal atoms from this cloud impinge on the specimen from all directions and condense evenly on it. The fine grained structure of the sputtered film depends on the target material, the working distance, the gas pressure and the sputtering current as well as of the process duration.

Chapter 5

5. Preparation and Characterization of Samples

In this work two types of samples were studied namely the F doped quaternary $SmO_{1-x}F_xFeAs$ (1111) compound and the ternary undoped $BaFe_2As_2$ and K doped $Ba_{1-x}K_xFe_2As_2$ (122) compound.

5.1 SmOFeAs (1111)

5.1.1 Polycrystalline Sample preparation for SmOFFeAs (1111)

These quaternary compounds were obtained by solid state reaction. The oxygen was introduced by powders of the transition metal oxide Fe_2O_3. The polycrystalline samples with nominal composition $SmO_{1-x}F_xFeAs$ (x=0.15, 0.175, 0.2) were synthesized by a two step solid state reaction in an evacuated quartz tube using high purity (≥ 99.95%) Sm, Fe, Fe_2O_3, As and SmF_3 powders as starting material. In the first step SmAs was obtained by reacting Sm and As at 600°C for 4 hours followed by 4 hours at 900 °C in a small Al_2O_3 crucible. Then the powder of Sm, SmF_3, Fe, As and Fe_2O_3 were accurately weighed according to the stoichiometric ratio of $SmO_{1-x}F_xFeAs$ (x=0.15, 0.175, 0.2). The weighed powders of raw material were mixed thoroughly and pressed into pellets. These pellets were placed into the Al_2O_3 crucible and then the crucible was placed into a quartz ampoule. The ampoules were sealed under argon atmosphere pumping and subsequently heated at 600°C for 4 hours and then 1150°C for 40 hours. Then the ampoule was cooled down slowly to room temperature. The sample preparation process except for annealing was carried out in glove box filled with pure argon atmosphere. Since the vapor pressure of elementary As is high at temperature greater than 600°C, it is important to avoid the explosion of sealed quartz ampoule during the main reaction. Here we used the quartz ampoule because the quartz material is durable for high temperatures and also provide the water free environment, which are important factors to avoid the explosion. The Ar gas filling in the ampoule was effective to prevent the collapse of the quartz ampoule during the heating procedure. Figure (5.1) shows the schematic diagram of quartz ampoule and the crucible.

The structure of $SmO_{1-x}F_xFeAs$ (x=0.1) was characterized by power X-ray diffraction (Bruker's X-Rays Diffraction D8) as shown in Figure (5.2). The XRD patterns indicate that all samples have a main phase of SmOFFeAs structure, which belongs to tetragonal ZrCuSiAs structure with a=0.3988 nm and b=0.8787 nm and some impurity phases. The impurity phases have been determined to be the known oxides, arsenide, and fluorides that were formed by starting chemicals, which do not superconduct at the measuring temperature. The impurity phases always exist due to the unbalance of the stoichiometry ratio and insufficient synthesis time. Figure (5.3) shows the energy dispersive X- ray microanalysis (EDS) spectrum of one typical grain from a polycrystalline sample. We can see from this spectrum that the main elements of this grain are Sm, F, Fe, As, and O. It is thus safe to conclude that the superconductivity observed here comes from the main phase of this element. A Scanning Electron Microscope image of our polycrystalline sample is presented in Figure (5.4)

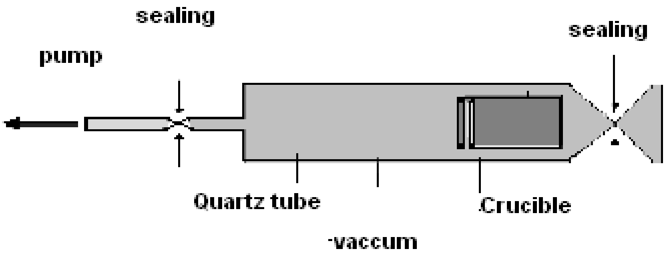

Figure (5.1): *Schematic diagram of quartz ampoule with crucible*

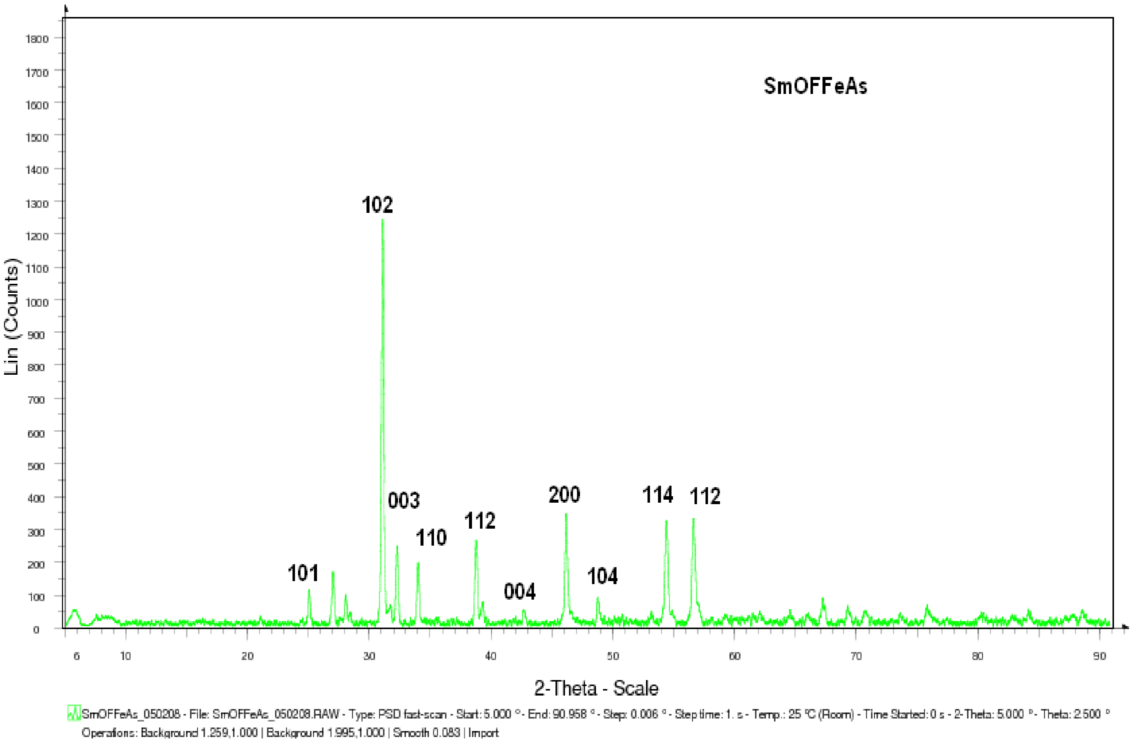

Figure (5.2): *X-ray diffraction pattern for the sample with nominal composition* $SmO_{1-x}F_xFeAs$ *(x=0.1) at 1150°. All main peaks can be indexed by tetragonal ZrCuSiAs structure.*

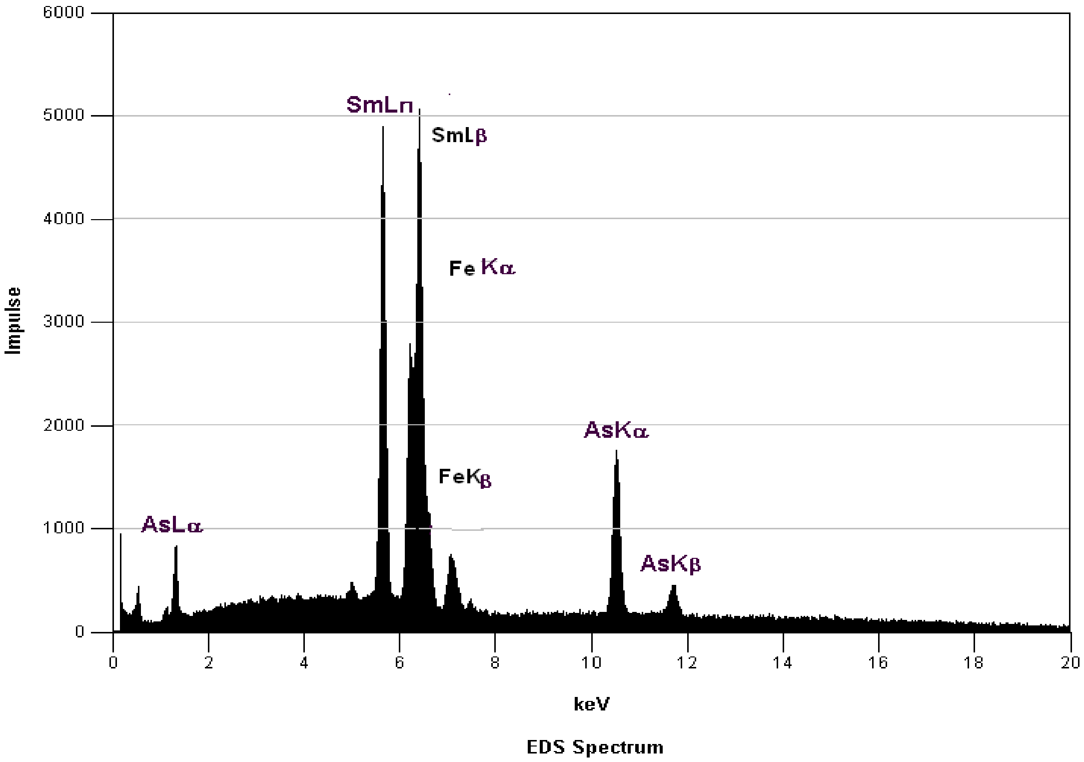

Figure (5.3): *Energy Dispersive Spectrum taken from one of the grains of* $SmO_{0.8}F_{0.2}FeAs$

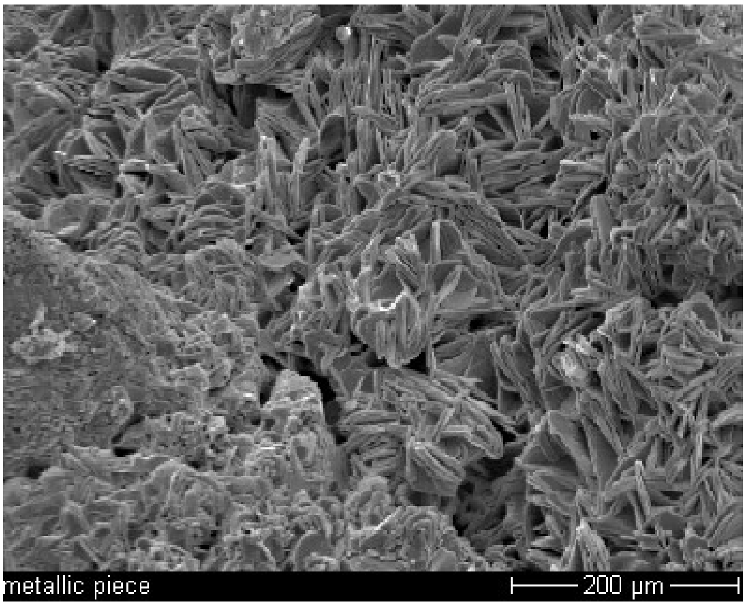

Figure (5.4a): *SEM image of a* F^- *doped polycrystalline sample of* $SmF_{0.2}O_{0.8}FeAs$.

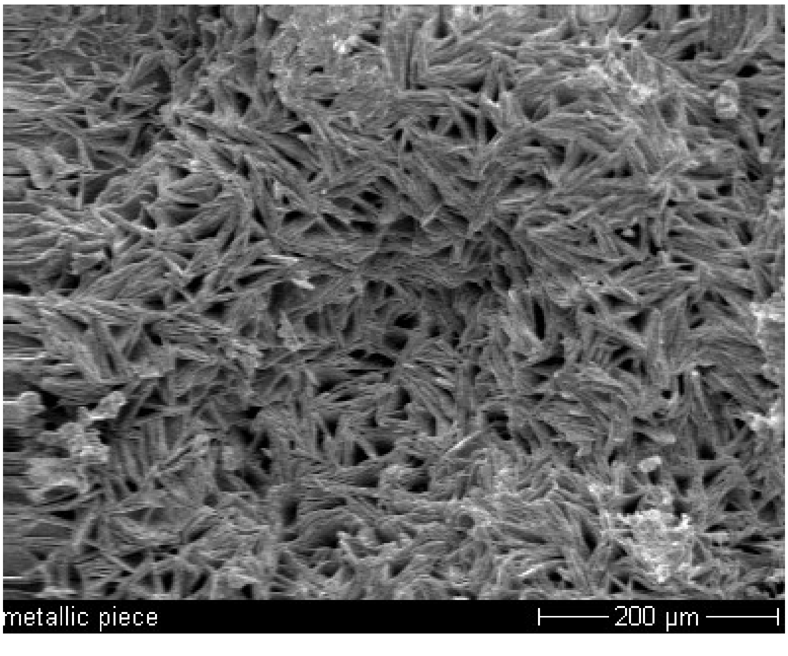

Figure (5.4b): *SEM picture of a polycrystalline sample of* $SmO_{0.8}F_{0.2}FeAs$

5.1.2 Transport measurement

In this work the temperature dependent electrical resistivity was measured, by the standard four point method under magnetic fields between 0T to 14T for different doped polycrystalline samples of $SmO_{1-x}F_xFeAs$. The results are shown in the following figures. The polycrystalline sample with fluorine doping x=0.1 is nonsuperconducting and a shows strong anomaly at an about 142K Figure (5.6). The resistivity drops steeply below 142K temperature and comes less pronounced. Superconductivity occurs when the anomaly was removed by electron doping of F^- as a substitution for O^{2-}. The doped electrons transfer to the FeAs layer to enhance the charge difference between the layers. When doping increased to x=0.15, the strong anomaly was suppressed and superconductivity appeared at T_c=18 Figure (5.7). For x=0.22K the T_c was 22K and finally the highest Tc=49 K for the x=0.2 was observed, which is shown in Figure (5.8). A broad transition would indicate significant doping variations. Figure 5.8b shows the temperature dependent resistivity for different magnetic field . The Inset in Figure (5.8b) shows the B-T phase diagram for $SmO_{1-x}F_xFeAs$ (x=0.2). The Superconducting transition temperature decreases linearly but slowly with increase in magnetic field.

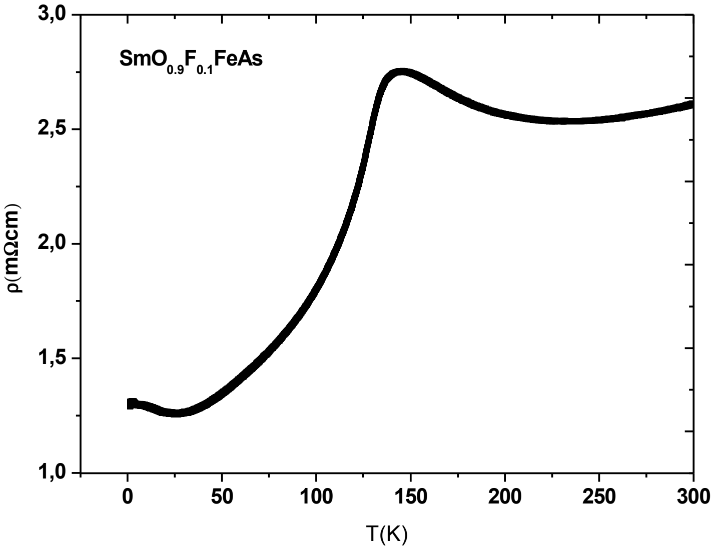

Figure (5.6):

Temperature dependent resistivity for polycrystalline $SmO_{0.9}F_{0.1}FeA$

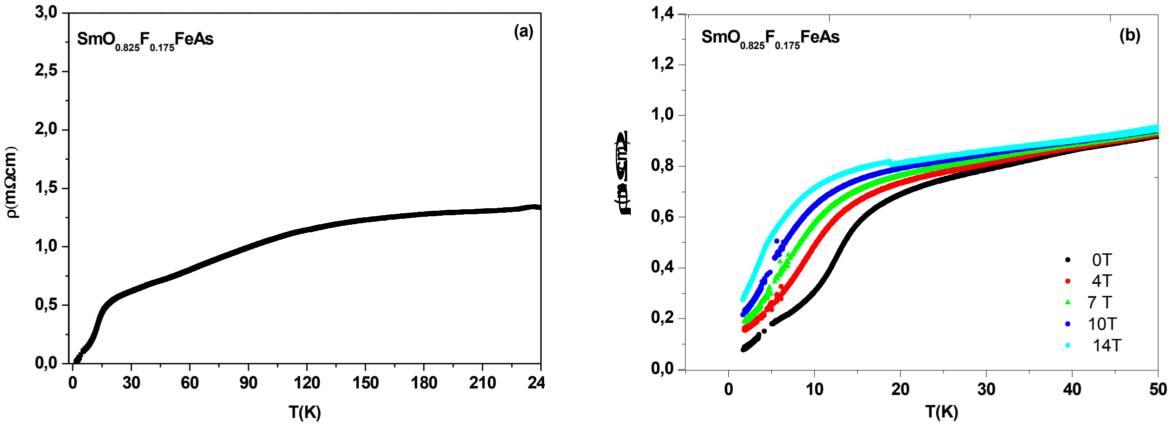

(a) **(b)**

Figure (5.7a & b): *The temperature dependent resistivity for* $SmO_{0.85}F_{0.15}FeAs$*. The black curve Figure (a)represents the zero field resistivity and Figure (b) represents the resistivity for different magnetic field.*

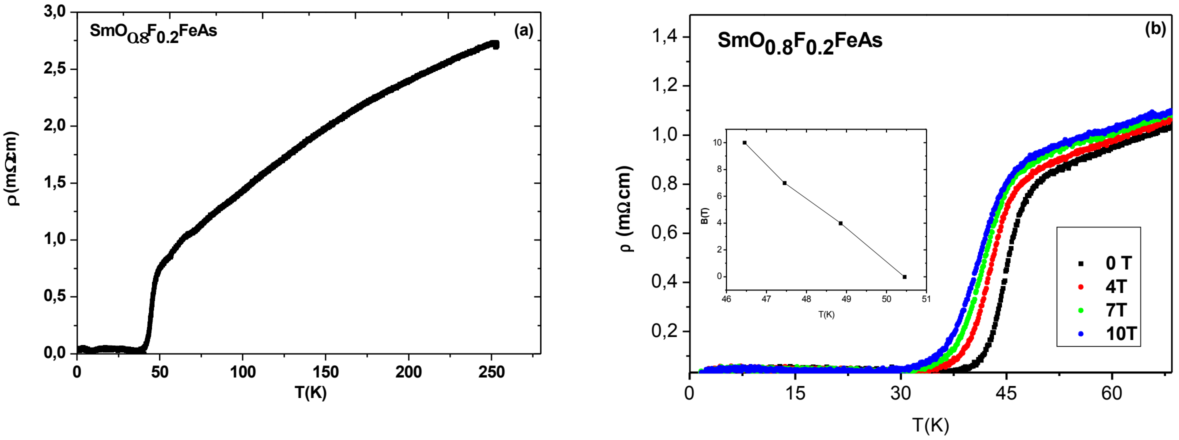

(a) **(b)**

Figure (5.8a & b) *shows the temperature dependent resistivity for* $SmO_{0.8}F_{0.2}FeAs$*. Figure (5.8a) shows the resistivity at zero magnetic field. And Figure (5.8b) shows the transition curves for different magnetic fields.*

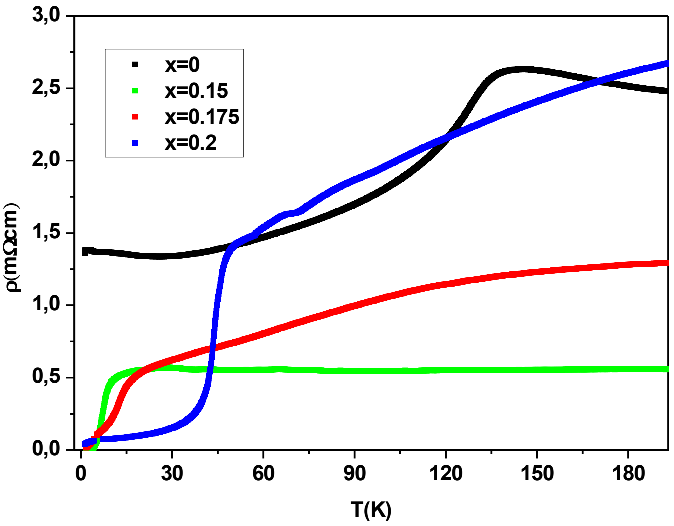

Figure 5.9*: Temperature dependent resistivity for different doping of SmO*$_{1}$*-xFxFeAs(x=0.1, 0.15, 0175, 0.2).*

The ac magnetization measurement was performed in a SQUID (Quantum Design MPMS-7T system). The magnetic characterization of the superconducting transition was done under zero magnetic fields. Data in Figure (5.10) shows a further confirmation of the superconducting transition temperature for the $SmO_{1-x}F_xFeAs$ (x=0.1, 0.15,0.175,0.2) polycrystalline samples.

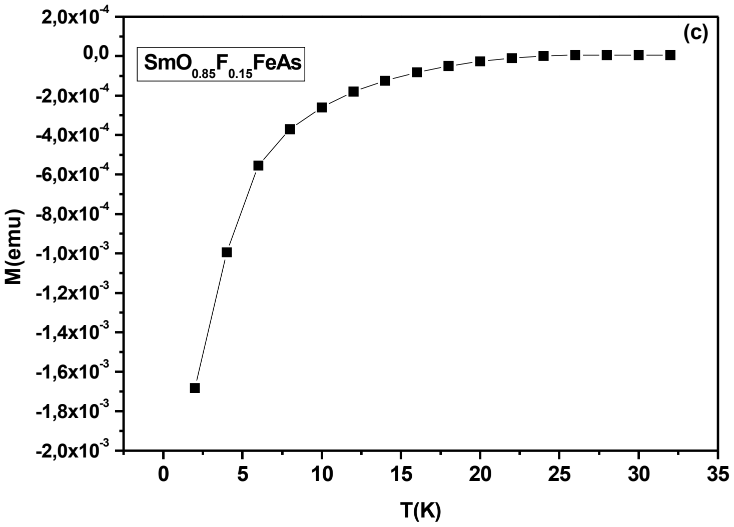

Figure 5.10 :*(a),(b),(c) shows the temperature dependent ac susceptibility for* $SmO_{1-x}F_xFeAs$ *for doping x=0.2, 0.175,0.15 respectively*

5.2 Ternary compound (122)

5.2.1 Sample preparation for $Ba_{1-x}K_xFe_2As_2$

Single crystals of AFe_2As_2 can be grown using two methods. One of those methods is with Sn flux and the other uses a self flux method. In this work we used the Sn flux method to grow the single crystals of $BaFe_2As_2$ and $Ba_{1-x}K_xFe_2As_2$, with conventional high temperature solution growth technique. Large crystals have been obtained in a homogeneous saturation. Pure Ba, K, Fe, and As were added into Sn flux in the stoichiometric ratio ($Ba_{1-x}K_xFe_2As_2$), where Sn :($Ba_{1-x}K_xFe_2As_2$) were to be 48:1. The compounds were placed into a 2ml Al_2O_3 crucible. The second smaller crucible we placed on top of that first crucible with silica wool on top of growth crucible and both were sealed in a quartz ampoule under 0.3 atmospheres of argon gas. For this experiment we prepared special quartz ampoule so that the second crucible can stay on top of the first one, during Sn decantation from the single crystals. Figure (5.11) shows the quartz ampoule with crucible.

All the procedures were performed in the glove box with the argon atmosphere. Then the sealed ampoule was placed into programmable electric furnace. The position of the furnace was kept vertical in direction shown in Figure (5.12(a)) and heated up to 850° C and cooled over a 40 hours. Once the furnace reached 500°C the furnace was turned as shown in Figure (5.12(b)) so the Sn flux could be decanted from the single crystals. After decanting, the temperature should be maintained at 500°C for 3 hours to get Sn free single crystals and then cooled to room temperature. For the mother compound the ampoule was heated up to 900°C and then cooled. After cooling, free standing single crystals were observed at the bottom of the crucible. When we exceeded the heating program up to 900°C for K doped samples, it was observed that there is less amount of K in the single crystals. It is necessary to use an excess of K to compensate the loss of K (due to high vapor pressure) from the stoichiometric ratio of $Ba_{1-x}K_xFe_2As_2$. These crystals are large and thin and it was easy to separate them. The approximate dimensions were few 1-2 mm × 1-2 and thickness ranges in 20 to 300μm. The c-axis is perpendicular to the platelet like of the single crystal. Figure (5.15) a and b shows SEM pictures of single crystals of $Ba_{1-x}K_xFe_2As_2$. ($x=0.45$).

The structure and phase purity of a grown crystals were identified by XRD (X ray diffraction). The XRD patterns were obtained using ground powders of as-grown single crystals. The results are shown in Figure (5.14) for the pure and doped $Ba1_{-x}K_xFe_2As_2$. The crystals belong to the tetragonal structure with space group *I*4*/mmm* at room temperature. These results are in agreement with the reported data [24]. From Figure (5.14), it is clear that most of the peaks can be indexed by tetragonal $ThCrSi_2As_2$ structure. Several peaks were that appeared on the graph were due to a impurity phase caused by Sn flux or K doping.

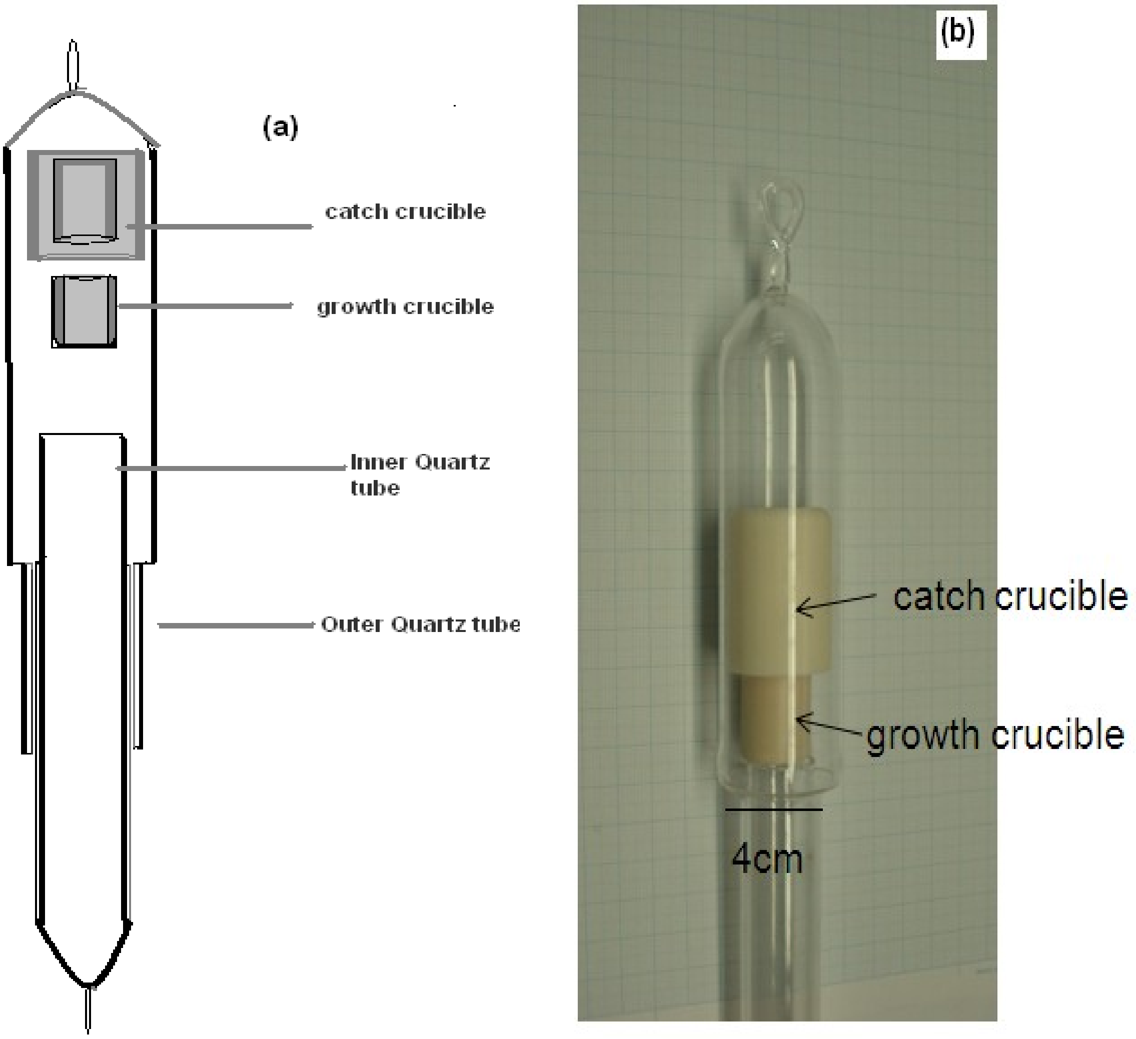

Figure 5.11: *(a) Schematic drawing of the quartz tube used for preparation of single crystals of $Ba1_{-x}K_xFe_2As_2$. (b) Picture of quartz tube*

***Figure 5.12**: (a) shows the initial position of electrical furnace. (b) Shows the decanting position of electrical furnace*

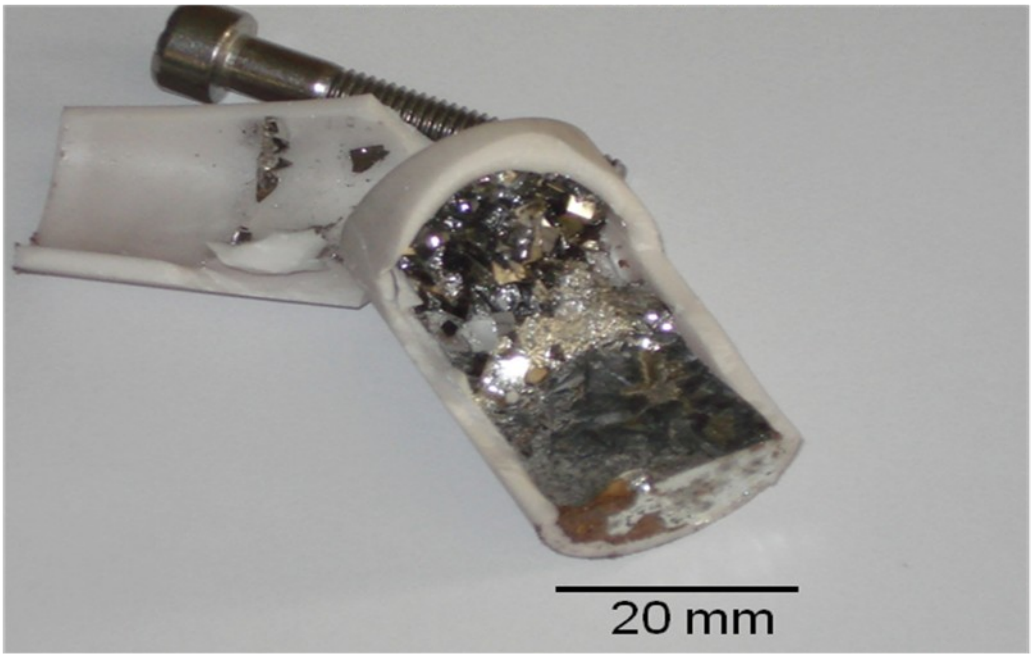

Figure 5.13: *Alumina crucible with single crystals at the bottom of the crucible and separated Sn flux*

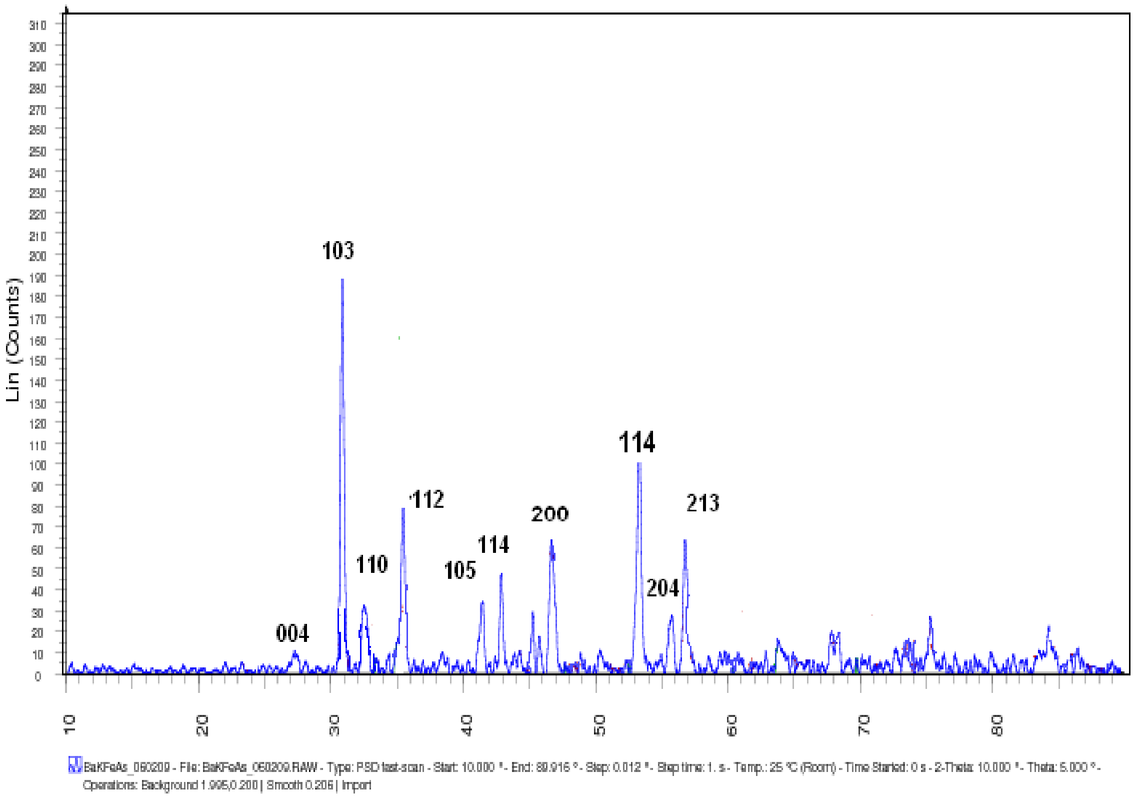

Figure 5.13: *The XRD diffraction Pattern for* $Ba_{0.55}K_{0.45}Fe_2As_2$ *Single Crystals (Single crystal prepared powder XRD Pattern).*

The chemical composition was determined by energy dispersive X-ray spectrometry (EDX) for the undoped parent compound $BaFe_2As_2$ and for the doped $Ba_{1-x}K_x Fe_2As_2$. From Figure (5.15), we can see that the peaks appeared in the spectra are mainly due to Ba, K, Fe, As which confirms that the superconductivity in the ternary compound is due to these elemental composition. The crystal morphology was studied by a scanning electron microscopy (SEM). SEM pictures shows the crystals are layered, with some Sn droplets on the surface of the single crystals. From pictures we can see some micro terraces and a bunch of steps on the crystal surface, which shows that these crystals were grown layer by layer. In the crystal the EDX analysis showed that the samples have a stoichiometric compositions ratio of about (Ba+K): Fe: As=1:2:2, with approximately 1% Sn appearing to be present as well. This confirms that Sn is not only present on the surface, but also that a small amount of Sn is incorporated in the structure of the sample. The elemental analysis in atomic % for different crystals from the same batch is shown in the following table.

No of samples	**Ba**	**K**	**As**	**Fe**	**Sn**
1.	6.90	10.17	42.05	39.66	1.22
2.	6.67	10.68	42.04	40.34	0.27
3.	10.95	4.48	42.16	41.37	1.04
4.	11.15	4.13	40.25	42.84	0.82

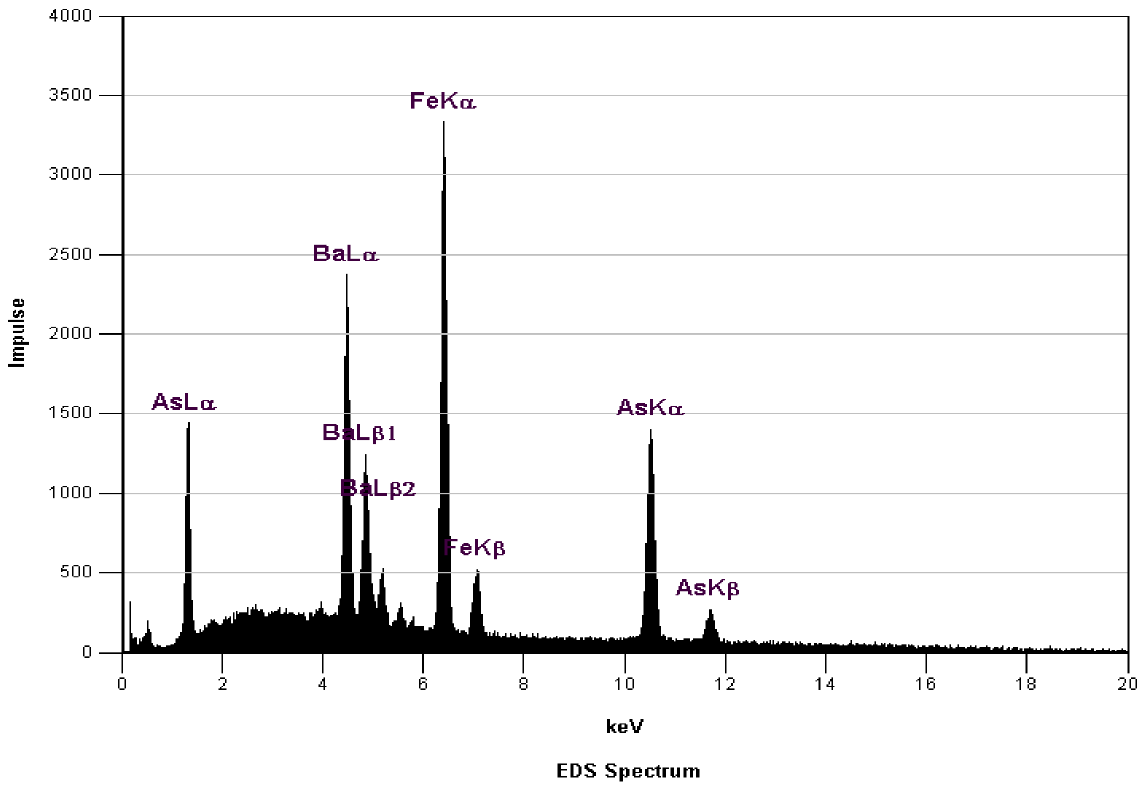

Figure 5.14: *Energy Dispersive Spectrum (EDS) for* $BaFe_2As_2$*. It shows the elements from the sample.*

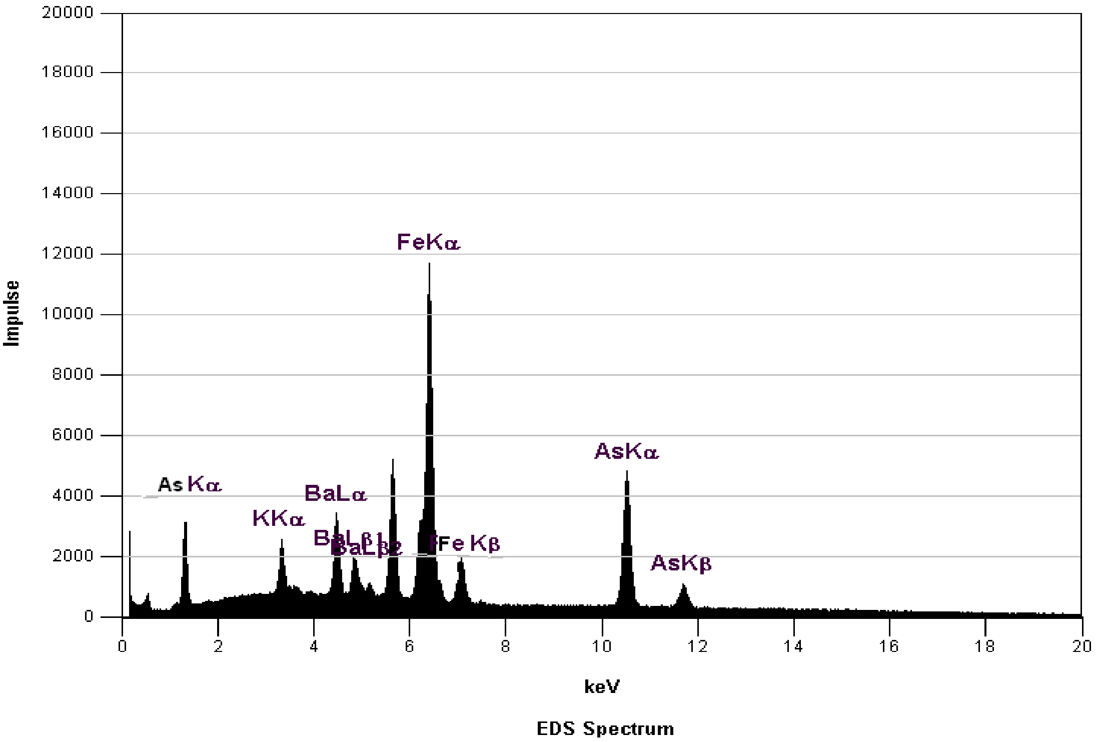

Figure 5.15**:** EDS spectrum for K doped $Ba_{0.55}K_{0.45}Fe_2As_2$ single crystal

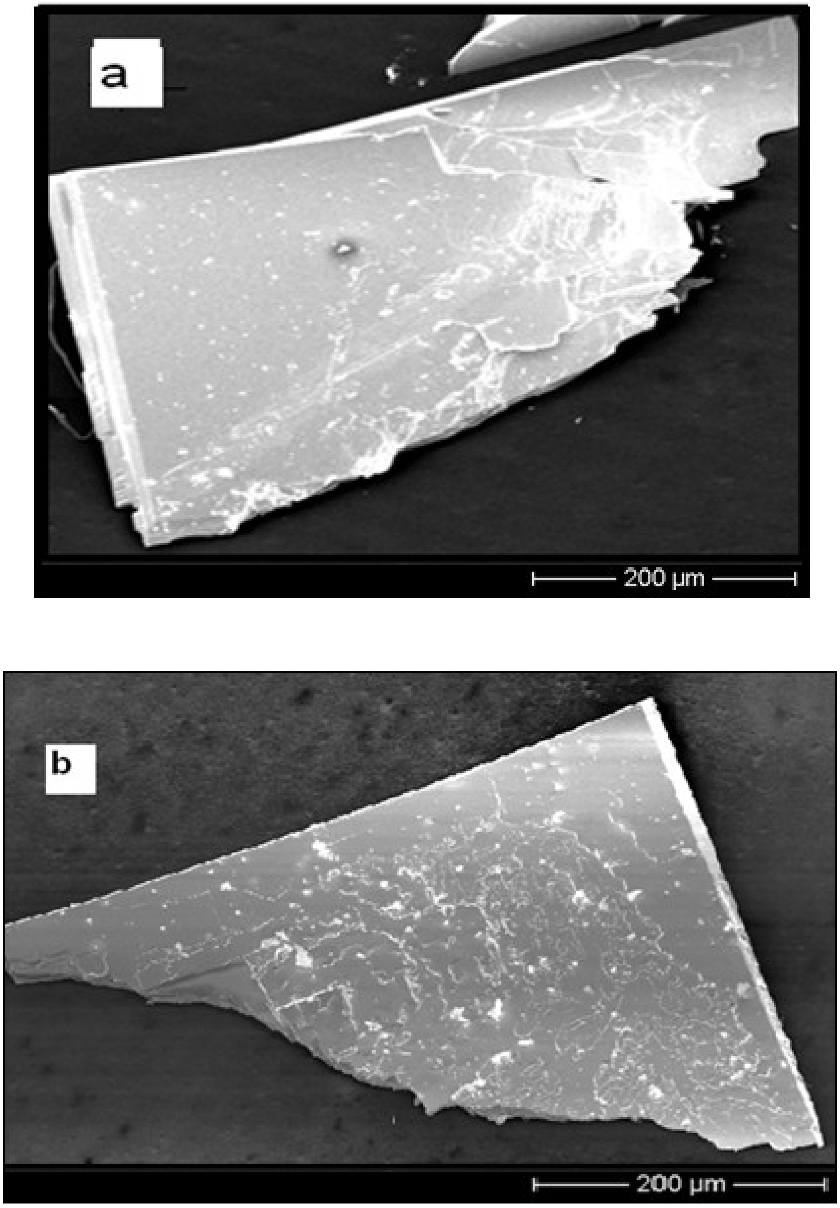

Figure 5.16: *Scanning electron microscopic (SEM) pictures of* $Ba_{1-x}K_xFe_2As_2$

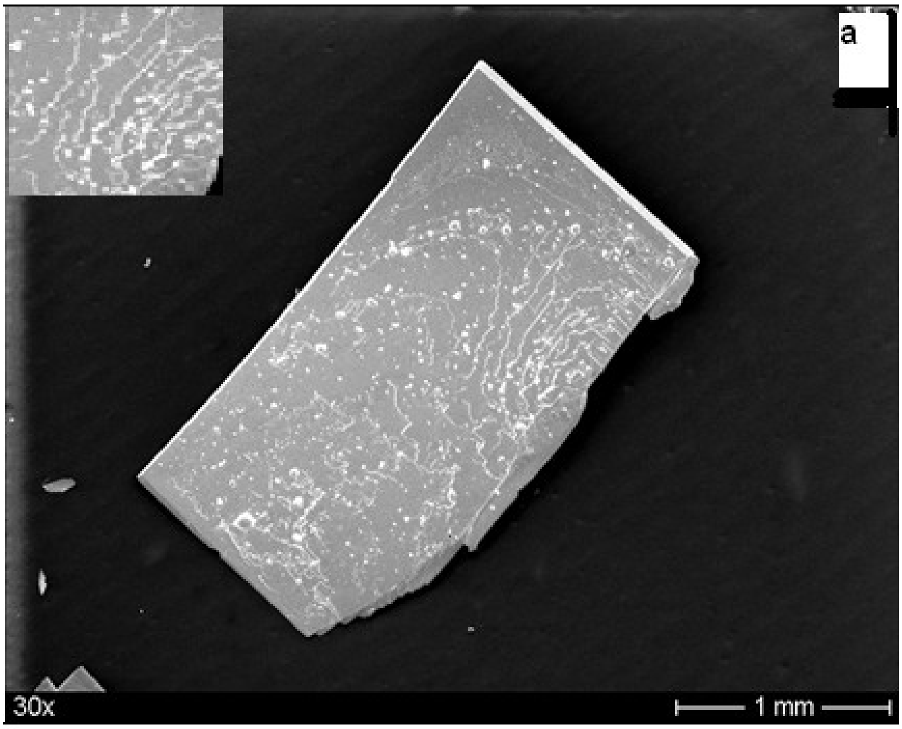
a
30x
1 mm

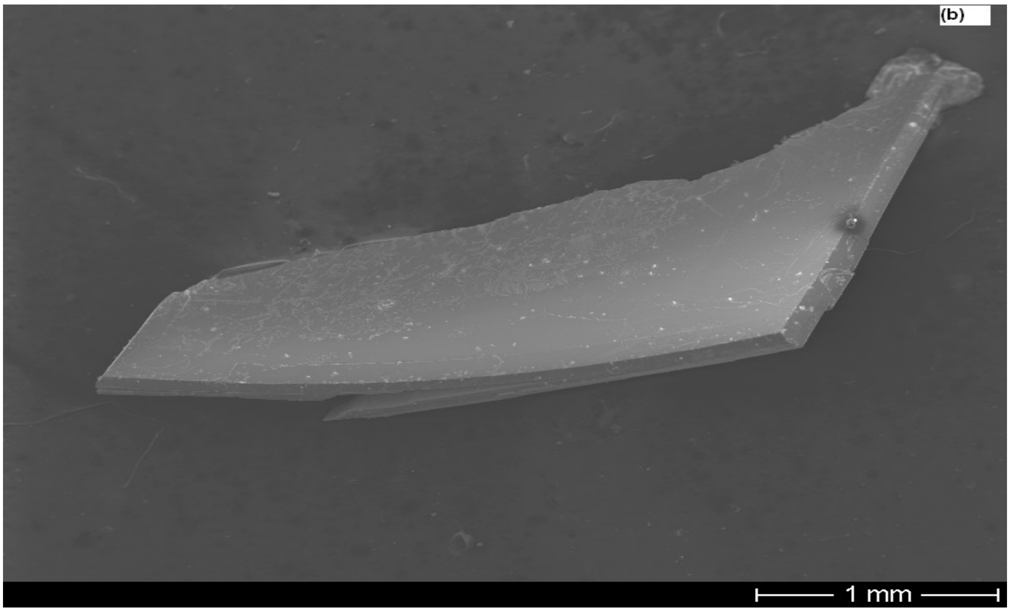
(b)
1 mm

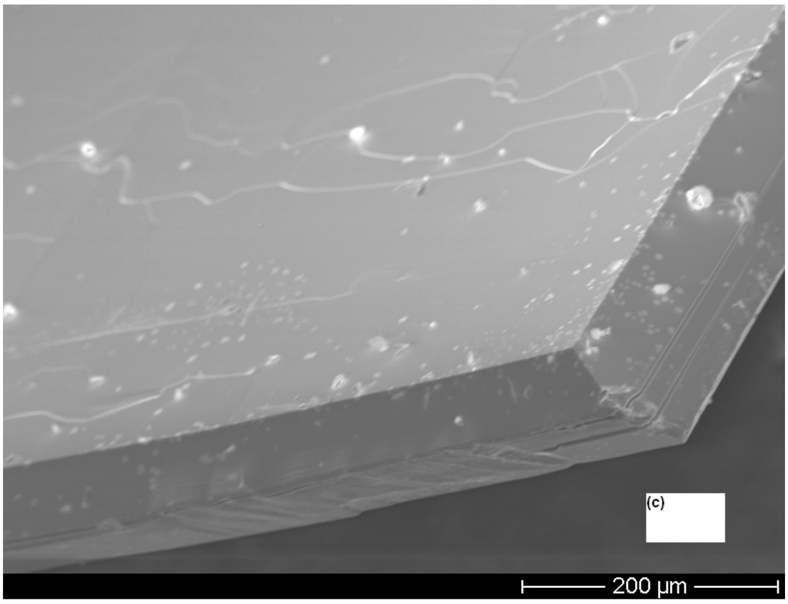

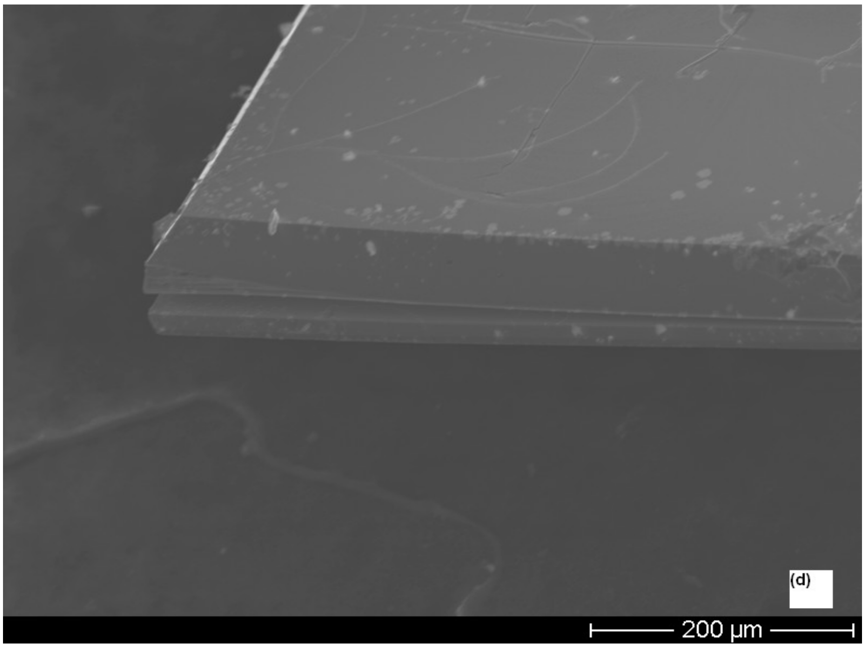

Figure 5.17**:** Figure (a) single crystal of $Ba_{0.55}K_{0.45}Fe_2As_2$, inset shows the micro steps on the surface of the crystal. The white dots are Sn droplets from the residual flux. Figure (b) ,(c),(d) shows a single crystal with curved surface and top layer It is partly cleaved off and separated along the *c axis.*

5.2.2 Transport properties

In this section of this work an overview is given about characteristic properties of the examined samples in c-axis transport measurements in magnetic fields up to 14T. The temperature dependence of in plane resistivity for single crystals was measured between 2 < T < 300K under different applied magnetic fields, for the single crystals of the parent compound $BaFe_2As_2$ and different K doped $Ba_{1-x}K_xFe_2As_2$ crystals.

Magnetic field and temperature dependent electrical transport data were collected using an Oxford cryogenic system. Resistivity values were determined by estimating the thickness of the sample with the help of high resolution microscopic images of single crystals. Hall measurements were performed using four point ac (f=300 Hz and I=1 to 5 mA) with current flowing in ab plane and applied magnetic field is perpendicular to the plane. The field is applied in two directions –H and +H. The Hall resistivity ρ_{xy} (B) was measured, from which the Hall coefficient R_H is obtained.

For the parent compound grown with Sn flux, the resistivity weakly depends on the temperature. The Figure (5.17) a and b shows the electrical resistivity data for $BaFe_2As_2$ crystals. From Figure (5.15) a we can see that, for 300 K > T >90 K the resistivity is relatively large and weakly temperature dependent. When cooled below 90 K the resistivity increases again and now the value of resistivity at 4K is almost double the previous value of resistivity at 90 K. The application of field perpendicular to c-axis does not showed any changes at 90 K. But it showed small change at lower temperature. Figure (5.17) a and Figure (5.17) b shows the temperature dependent resistivity for two different crystals with different dimensions from the same batch. Both figures show the decrease in resistivity at same temperature at 90 K. Figure (5.17) b shows that when sample is cooled to 1.5 K the crystal showed evidence of superconductivity at 1.8K with 0T field. When we applied the magnetic field, the superconductivity disappeared. This superconductivity at low temperature might be because of the small amount of Sn present inside the sample. (Elementary Sn has a transition temperature 3.7 K).

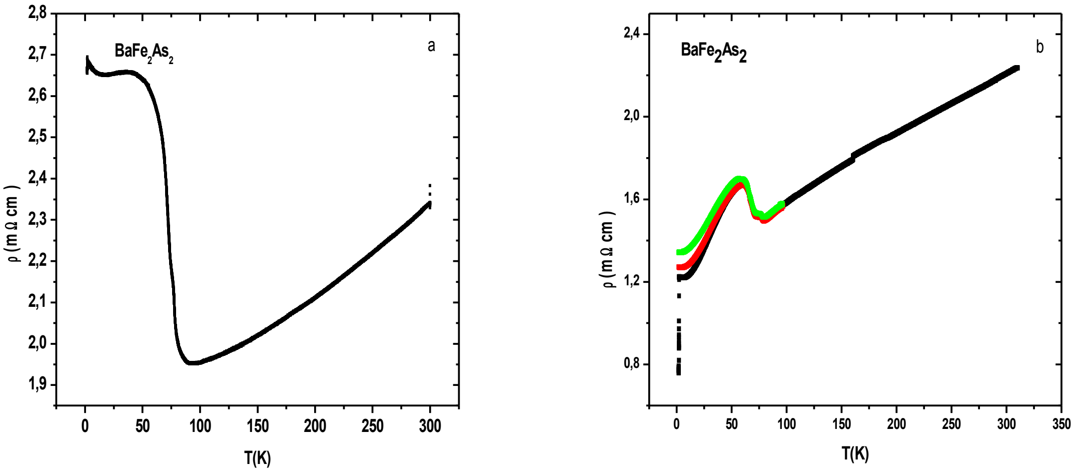

Fig5.17: *Figure (a)and Figure (b) shows the temperature dependent resistivity for the two different single crystals from the same batch, Figure (a) shows the curve with zero magnetic field and Figure b shows the resistivity curve with zero magnetic field (black curve) and with different magnetic field up to 100K Temperature.*

Temperature dependent electrical resistivity data of K doped $Ba_{1-x}K_xFe_2As_2$ samples was measured for different samples from the same batch with different size and thickness both are shown in Figure (5.18) and Figure (5.19). Both crystals have shown the similar result. For this compound superconductivity appears at temperature of Tc=23 K with huge bump at 75K. For these samples the resistivity drops at 75 K dramatically (like in the parent compound, which shows the phase transition at 90 K) and then increases till 23K where it drops again to show superconductivity, which is very different from the other reports. In this work we measured two crystals from the same batch. Both crystals showed sharp superconducting transition at 23K. This transition was consistent on application of 14T magnetic field. The bump at 75 K may be induced by the inhomogeneous phase formed during the reaction.

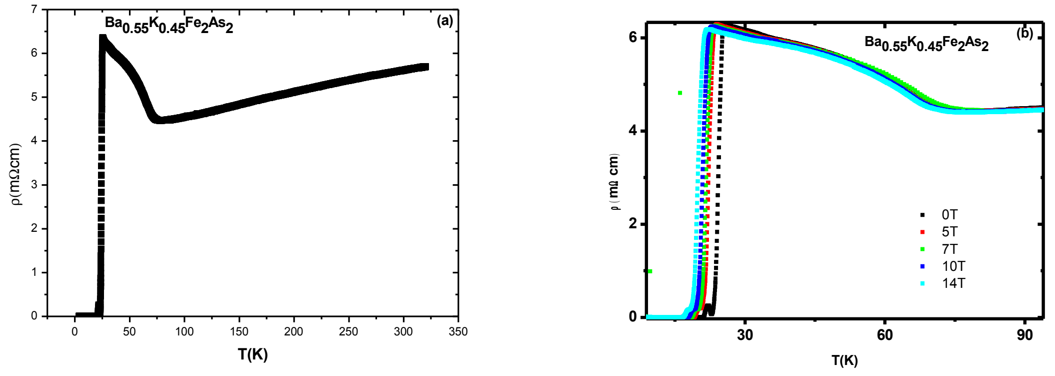

Figure 5.18: *Temperature dependent resistivity curve for* $Ba_{1-x}K_xFe_2As_2$ *(x=0.45)*

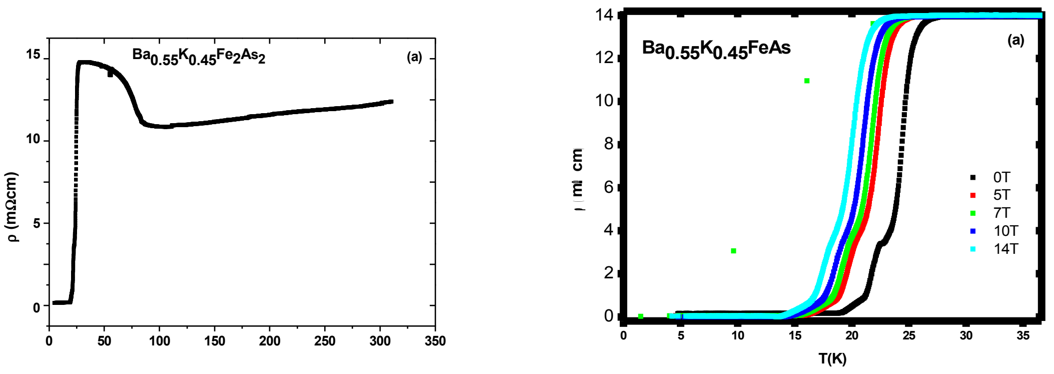

Fig5.19*: Temperature dependent resistivity curve for* $Ba_{1-x}K_xFe_2As_2$ *(x=0.45)*

The ac magnetization data in Figure (5.20) measured by SQUID magnetometer shows a further confirmation of the superconducting transition temperature T_c~*23 K* for the $Ba_{0.55}K_{0.45}Fe_2As_2$ single crystal.

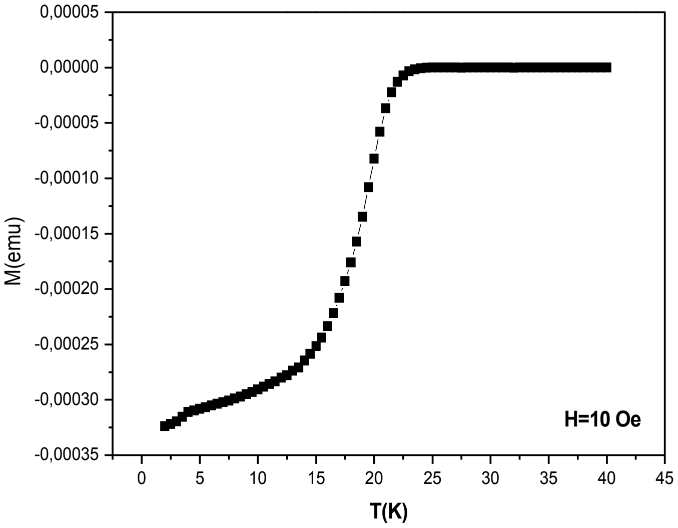

Figure 5.20: *Temperature dependent ac magnetization for* $Ba_{0.55}K_{0.45}Fe_2As_2$

To get the comprehensive understanding to conducting carriers In $Ba_{0.55}K_{0.45}FeAs$ phase, we measured the hall effect of the above sample. Figure 5.21 shows the magnetic field dependence of the transverse resistivity (ρ_{xy}) at different temperatures. In the experiment, ρ_{xy} was taken as

$\rho_{xy} = [\rho(+H) - \rho(-H)]/2$, ($\rho(H) = \rho_{xx}(H) + \rho_H$)

at each point to eliminate the effect of the misaligned Hall electrodes. It is important to note here that, when transverse measurement are done across the sample a certain longitudinal signal is superimposed onto the transverse voltage as a longitudinal misalignment. The longitudinal resistivity ρ_{xx} is symmetric with respect to the field direction. Such as $\rho_{xx}(H) = \rho_{xx}(-H)$. Whereas the Hall resistivity ρ_H is antisymmetric. Therefore, one can take advantage of symmetry to cancel the effect of the longitudinal signal and extract only the Hall contribution. This antisymmetrization procedure is necessary in order to extract the weak transverse voltage signal from the total of the measured signal.

The Figure (5.21) shows the raw data of the transverse resistivity ρ_{xy} at different temperature, which is in good linear relation against the magnetic field. The transverse resistivity (ρ_{xy}) are all positive indicating that hole like charge carriers. The temperature dependence of the Hall coefficient R_H is presented in the Figure (5.22), which decays continuously with increasing temperature. One can see from the Figure (5.22), R_H remains positive in a wide temperature regime and it is strong temperature dependent. This estimation is based on a single band model.

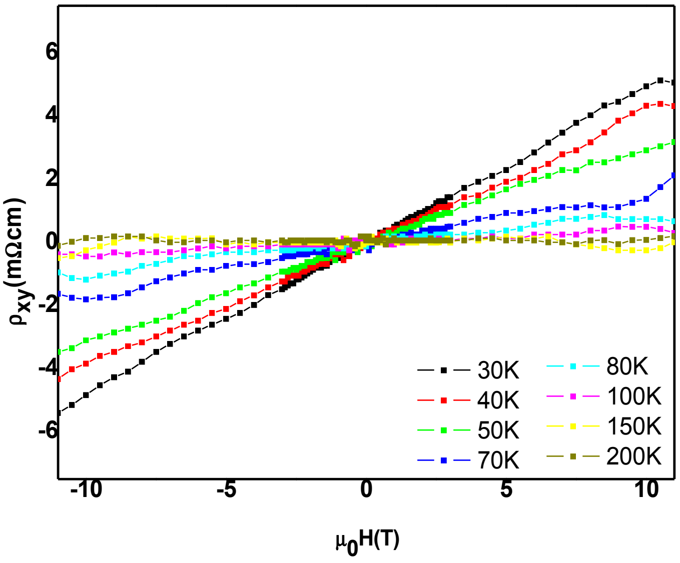

Fig5.21: *Relation between transverse resistivity* ρ_{xy} *and magnetic field at different temperatures for* $Ba_{0.55}K_{0.45}Fe_2As_2$*.*

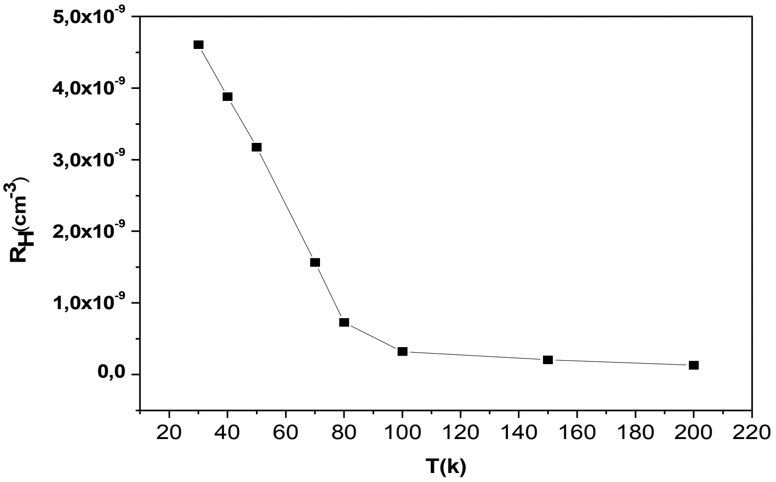

Fig5.22: *Temperature dependence of the Hall coefficient* R_H *for the superconducting sample* $Ba_{0.55}K_{0.45}Fe_2As_2$*.*

From the above Figure (5.18) and (5.19), we can see that the phase transition is not completely suppressed in the doped samples. To study the thermal behavior of the single crystals of $Ba_{1-x}K_xFe_2As_2$ (x=0.45), we did the thermogravimetric and differential thermal analysis on this samples. A tiny crystal of $Ba_{1-x}K_xFe_2As_2$ (x=0.45) was loaded in a small alumina crucible and then heated to the maximum temperature. .But result had shown the continuous decomposition of sample with loss of As and K.

To cope up of this problem, we extended the cooling time for several hours. For the new batch of $Ba_{1-x}K_xFe_2As_2$ (x=0.45) samples, we used the excess K in the new batch of sample. The Ba, K, Fe, As and Sn was mixed together as $Ba_{1-x}K_xFe_2As_2$ (x=0.45) in the ratio 1:48 and then this compound was heated up to 850°C for 8 hours subsequently, then temperatures were decreased to ~600°C at a low cooling rate of 3K/h. and cooled over 90 hours to 500° C. For this temperature, the crystal quality and transition temperature were improved.

The temperature dependent resistivity data is shown in following Figure (5.23). For this single crystal sharp superconducting transition occurs at T_c~27 K. The phase transition at 70 K, which was observed in the previous K^+ doped samples with average composition of $Ba_{0.55}K_{0.45}Fe_2As_2$ was suppressed in the new batch of sample. Figure 5.23b shows the electrical resistivity data ρ (T) in presence of different magnetic fields. As clear from the figure, with increase in magnetic field the onset of superconducting temperature shifts towards lower temperature. Inset in Figure 5.23b shows the B-T phase diagram for $Ba_{0.55}K_{0.45}Fe_2As_2$ based on resistivity measurements. The Superconducting transition temperature decreases linearly but slowly with increasing magnetic field.

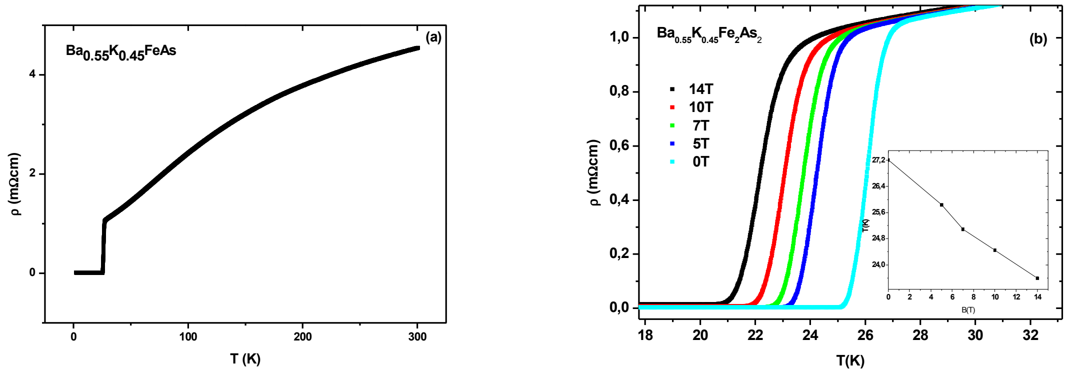

Fig5.23: *Temperature dependent resistivity of* $Ba_{0.60}K_{0.65}Fe_2As_2$. *The inset (b) shows the B-T Curve*

The temperature dependent ac magnetization susceptibility was measured with a modulationfield in amplitude of 10 G. The data in Figure (5.24) shows a further confirmation of the superconducting transition temperature Tc~27 K for the $Ba_{0.55}K_{0.45}Fe_2As_2$ single crystal out of the same batch.

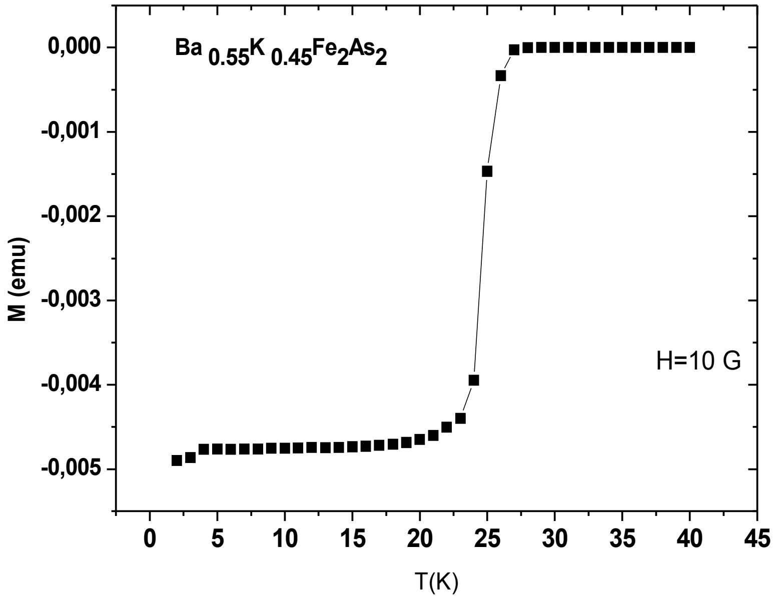

Figure 5.24: *temperature dependent ac SQUID magnetization curve for* $Ba_{0.55}K_{0.45}Fe_2As_2$

Chapter 6

6. Discussion

The whole work is dedicated to the synthesis and the study of physical properties of the quaternary oxypnictides and oxygen free ternary iron arsenide superconductors.

These materials are comparatively new class of High Temperature Superconductors. Although a lot of theoretical work has been done on this class of high temperature superconductors since one year, the mechanism of the superconductivity is still not clear for these compounds.

This work describes the synthesis of polycrystalline samples with nominal composition of $SmO_{1-x}F_x$ FeAs (x= 0.1, 0.15, 0.175, 0.2). The polycrystalline sample of $SmO_{1-x}F_x$ FeAs (x=0.1) did not show superconductivity rather it showed the SDW phase transition at 142 K, which is similar to the other reports, which showed the phase transition at 150K.. When doping was increased to x=0.15 the phase transition was suppressed and the transition temperature was observed at 18K. Initially at small doping there was a broad transition. This difference decreased with higher doping. The transition temperature increased with increasing doping and at x=0.2 the highest onset Tc was found to be 50K and zero resistivity transition was found at Tc=46K.

To study the superconductivity, electrical and magnetic behavior of these new compounds, single crystals would be favorable. Unfortunately growth of single crystals of these quaternary oxypnictide is proven to be difficult. On the other hand in oxygen free ternary (122) the single crystals were relatively easy to grow. Therefore we concentrated more on ternary iron arsenide $Ba_{1-x}K_xFeAs$ superconductors.

The single crystals of these ternary iron arsenide $Ba_{1-x}K_xFeAs$ can be grown with two methods namely the self flux method and the Sn flux method. We have grown the single crystals from Sn flux.

Growth of single crystals of pure $BaFe_2As_2$ and doped $Ba_{1-x}K_xFeAs$ out of Sn flux provides us with nice few mm large single crystals. The parent compound showed a transition at 90K rather than 140 which is reported for polycrystalline sample parent compound ref. (15). Our result is similar to the ref (24). In this ref they observed the phase transition at 85K. The collected the X ray diffraction data on the $BaFe_2As_2$ shows the splitting of reflection at temperature 85 K. While there is no change below this temperature, this change at 85K is consistent with tetragonal to orthorhombic transition. As our crystals are grown by Sn flux and they contain 0.5 to 1% of Sn. This discrepancy of phase transition comparatively at lower temperature was due to small amount of Sn incorporated in to crystals during the crystal growth in Sn flux method. It might be possible that this effect is associated to the FeAs layer because the small amount of Sn substitutes Fe ions during crystal formation in a Sn melt. It is possible because the ionic radius of Fe^{2+} (0.78 Å) is nearly close to the ionic radius of Sn^{2+} (0.93 Å) while the ionic radius of Ba^{2+} is (1.42 Å).ref (46). The doping of K suppresses the spin density wave and induces superconductivity in $Ba_{0.55}K_{0.45}Fe_2As_2$

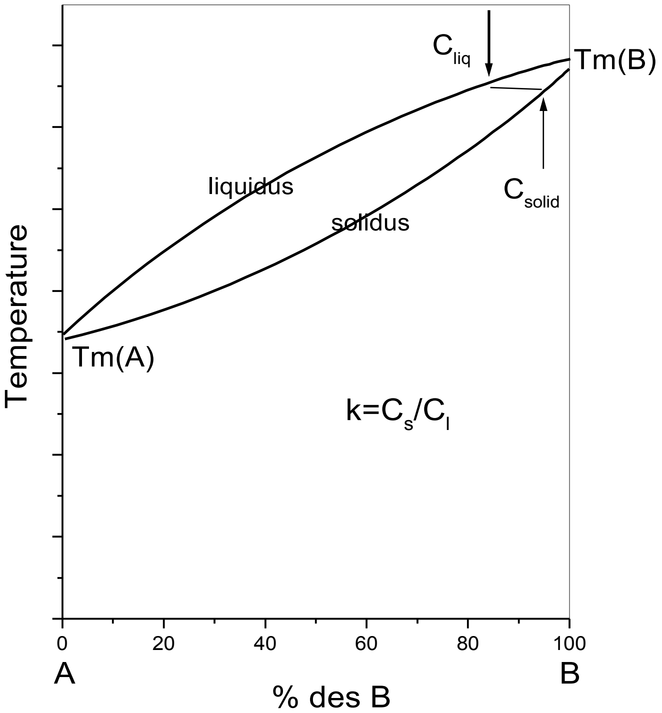

Figure 6.1: *shows the phase diagram*

If we consider the phase diagram of $Ba_{1-x}K_xFe_2As_2$ compound, one can probe the whole phase diagram with one sample. We can see from above Figure (6.1) the distribution coefficient k= C_s/C_l is not equal to 1 and we have a concentration gradient problem. The concentration gradient describes how the concentration of potassium changes from one place to another.

When we heated the compound of $Ba_{1-x}K_xFe_2As_2$ (x=0.45), the compound is in the liquid phase at maximum temperature of 1150°C. When it starts to cool down the liquid phase of compound moves towards the solid phase. As this compound grows layer by layer, in thE nucleation stage a small nucleus containing the newly forming crystal is created. Nucleation occurs relatively slowly as the initial crystal components must "bump" into each other in the correct orientation and place for them to form the crystal. Crystal growth spreads outwards from the nucleating site. In this faster process, the elements which form the motif add to the growing crystal on a prearranged system, and form the crystal lattice. Figure (6.1) shows that if these melted compound get solidified at higher temperature due to concentration gradient the less amount K was incorporated inside the single crystals. . The first nucleation occurs at higher temperature hence there is less amount of K present inside the crystals. These crystals grow outwards from nucleating site. The crystal growth along (*001*) face occurs at a relatively high super saturation according to two-dimensional nucleation, layer-by-layer growth mechanism. At lower temperature the concentration of potassium is higher. So the crystal grows with less amount K in the middle part of the crystal. So the composition of middle part is almost like the parent compound $BaFe_2As_2$, while on the surface and towards the edges of crystal the amount of K increases so the surface of the crystal has a concentration like the optimally doped compound.

And though the ionic radius of K (1.51 Å)) is bigger than Ba (1.42 Å), the growth rate along the(010) is faster than the (001) direction and the lattice constant of Ba is bigger than K along (001) and due to this there is an expansion of the lattice parameter. And the layers dislocate from each other due to internal stress at the edges of the crystal and looks like cleaved layers at the edges of the crystals .The SEM image in Figure (6.2) shows the cleaved edges single crystals of $Ba_{1-x}K_xFeAs$ (x=0.45).

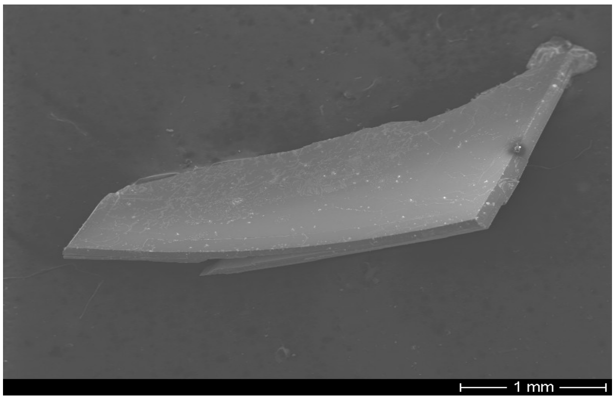

Figure 6.2: *cleaved layers of single crystal* $Ba_{1-x}K_xFe_2As_2$ *(x=0.45).*

Due to crucible growth these compounds lead to intrinsically inhomogeneous single crystals. These crystals grown by Sn flux method are highly sensitive to incorporation of Sn in to these samples. While in self flux method due to high vapor pressure of potassium (K) and high growing temperature there is a possibility of explosion of quartz container during growth of single crystals. From this we can see that it is challenging to grow a nice homogeneous single crystals with above describe method. There is need to think about another method to solve this concentration gradient problem.

References

7. References

[1] Y. Kamihara, T. Watanabe, M. Hirano, H. Hosono. J. Am. Chem. Soc. 130, 3296 Iron-Based Layered Superconductor La[$O_{1-x}F_x$]FeAs (x = 0.05-0.12) with T_c = 26 K (2008).

[2]Y. Kamihara ,T. Watanabe, M. Hirano, H. Kamiya Structural properties and phase transition of RFeMO (R=La, Nd; M=As, P) materials H2006 J.Am.Chem Soc: 128,10012

[3] G.F. Chen, Z. Li, G. Li, J. Zhou, D. Wu, J. Dong, W.Z. Hu, P. Zheng, Z.J. Chen, J.L. Luo, N.L. Wan : Superconducting properties of Fe-based layered superconductor LaO0.9F0.1−_FeAs: arXiv: 0803.0128.(2008)

[4] T. Nomura1, S. W. Kim, Y. Kamihara, M. Hirano, P. V. Sushko, K. Kato, M. Takata, A. L. Shluger and H. Hosono: Crystallographic Phase Transition and High-Tc Superconductivity in LaFeAsO:F: arXiv:0804.3569v2(2008)

[5] Zhi-An Ren, Guang-Can Che, Xiao-Li Dong, Jie Yang, Wei Lu, Wei Yi, Xiao-Li Shen, Zheng-Cai Li, Li-Ling Sun, Fang Zhou, Zhong-Xian Zhao: Superconductivity and Phase Diagram in Iron-based Arsenic-oxides $ReFeAsO_{1-d}$ (Re = rare earth metal) without Fluorine Doping: Europhys. arXiv: 0804.2582. (2008);

[6] Zimmer B I, Jeitschko W, Albering J H, Glaum R and Reehuis M 1995 *J. Alloys Compd.* **229** The rate earth transition metal phosphide oxides LnFePO, LnRuPO and LnCoPO with ZrCuSiAs type structure.

[7] Z. A. Ren, W. Lu, J. Yang, W. Yi, X.L. Shen, Z.C. Li, G.C. Che, X.L. Dong, L.L. Sun, F.Zhou, Z.X. Zhao, Chin. Phys. Lett. Superconductivity and phase diagram in iron-based arsenic-oxides $ReFeAsO_{1-\delta}$ (Re = rare-earth metal) without fluorine doping
25, 2215 (2008).

[8] Q. Huang, Jun Zhao, J. W. Lynn, G. F. Chen,J. L. Luo,N. L. Wang,3and Pengcheng Dai:, Doping evoluton of antiferromagnetic order and structural distortion in LaFeAsO1−xFx. arXiv:0809.4816v2(2008)

[9]Zhi-An Ren, Guang-Can Che, Xiao-Li Dong, Jie Yang, Wei Lu, Wei Yi, Xiao-Li Shen, Zheng-Cai Li, Li-Ling Sun, Fang Zhou, Zhong-Xian Zhao. Superconductivity and Phase Diagram in Iron-based Arsenic-oxides ReFeAsO1-d (Re = rare earth metal) without Fluorine Doping: arXiv:0804.2582 (2008).

[10] G.F. Chen, Z. Li, G. Li, J. Zhou, D. Wu, J. Dong, W.Z. Hu, P. Zheng, Z.J. Chen, J.L. Luo, N.L. Wang. arXiv: 0803.0128

[11] Xiyu Zhu, Huan Yang, Lei Fang, Gang Mu, Hai-Hu Wen. Supercond. Sci. Technol. 21, 105001 (2008); arXiv: 0803.0128

[12] A.S. Sefat, M.A. McGuire, B.C. Sales, Rongying Jin, J.Y. Howe, D. Mandrus. ; arXiv: 0803.2528(2008)

[13] X.H. Chen, T. Wu, G. Wu, R.H. Liu, H. Chen, D.F. Fang. Nature 453, 761 (2008); arXiv: 0803.3603(2008)

[14] G.F. Chen, Z. Li, D. Wu, G. Li, W.Z. Hu, J. Dong, P. Zheng, J.L. Luo, N.L. Wang. Phys. Rev. Lett. 100, 247002 (2008);arXiv: 0803.3790(2008)

[15] M. Rotter, M. Tegel, D. Johrendt. Phys. Rev. Lett 101, 107006 (2008); arXiv: 0805.4630.(2008)

[16] Krellner, C.etal. Magnetic and structural transitions in layered FeAs systems: AFe_2As_2 versus RFeAsO compounds. arXiv:0806.1043 (2008).

[17] Chen, G. F. et al. Superconductivity in hole-doped $(Sr_{1-x}K_x)Fe_2As_2$. arXiv:0806.1209 (2008).

[18] D. J. Singh, M. H. Du, LaFeAsO1−xFx: A low carrier density superconductor near itinerant magnetismarXiv:0803.0429

[19] I. A. Nekrasov, Z. V. Pchelkina, M. V. Sadovskii .Electronic Structure of Prototype AFe2As2 and ReOFeAs High-Temperature Superconductors: a Comparisonarxiv:0806.2630v2 ,(2008)

[20] Fermi surface nesting induced strong pairing in iron-based superconductors K. Terashima1, Y. Sekiba, J. H. Bowen, K. Nakayama, T. Kawahara, T. Sato, P. Richard, Y.-M. Xu, L. J. Li, G. H. Cao, Z.-A. Xu, H. Ding,and T. Takahashi : arXiv:0812.3704

[21]Fermi surface and strong coupling superconductivity in single crystal NdFeAsO1T xFx C. Liu, T. Kondo, M. E. Tillman, R. Gordon, G. D. Samolyuk, Y. Lee, C. Martin, J. L. McChesney, S.Bud'ko, M. A. Tanatar, E. Rotenberg, P. C. Can_eld, R. Prozorov, B. N . Harmon, and A. Kaminski: Fermi surface and strong coupling superconductivity in single crystal NdFeAsO1-xFx arXiv: 0806.2147

[22] Lin Zhao1, Haiyun Liu1, Wentao Zhang1, Jianqiao Meng1, Xiaowen Jia1, Guodong Liu1, Xiaoli Dong1, G. F. Chen, J. L. Luo, N. L. Wang, W. Lu, Guiling Wang, Yong Zhou, Yong Zhu, Xiaoyang Wang, Zuyan Xu, Chuangtian Chen, and X. J. Multiple Nodeless Superconducting Gaps in (Ba0.6K0.4)Fe2As2 Superconductor from Angle-Resolved Photoemission Spectroscopy :arXiv:0807.0398v2

[23]H. Ding, P. Richard, K. Nakayama, T. Sugawara, T. Arakane, Y. Sekiba, A. Takayama, S. Souma, T. Sato, T. Takahashi, Z. Wang, X. Dai, Z. Fang, G. F. Chen1, J. L. Luo1, and N. L. Wang: Observation of Fermi-surface-dependent nodeless superconducting gaps in Ba0.6K0.4Fe2As2 arXiv: 0807.0419

[24]N. Ni, S. L. Bud'ko, A. Kreyssig, S. Nandi, G. E. Rustan, A. I. Goldman, S. Gupta, J. D. Corbett, A. Kracher, and P. C. Canfield Ames Laboratory US DOE, Iowa State University, Ames, Iowa 50011, Anisotropic thermodynamic and transport properties of single crystalline (Ba1−xKx)Fe2As2 (x = 0 and 0.45). arXiv: 0806.1874v2

[25] H. Chen, Y. Ren, Y. Qiu, Wei Bao, R. H. Liu, G. Wu, T. Wu, Y. L. Xie,1X. F. Wang, Q. Huang and X. H. Chen. Coexistence of the spin-density-wave and superconductivity in the $Ba_{1-x}K_xFe_2As_2$

[26] Alireza P. L., Ko Y T C,Gillett J, J.Phys.: condens matter 21 012208

[27]Patricia L. Alireza, Y. T. Chris Ko, Jack Gillett, Chiara M. Petrone, Jacqueline M. Cole, Suchitra E. Sebastian1, and Gilbert G. Lonzarich. Superconductivity up to 29 K in SrFe2As2 and BaFe2As2 at high pressures arXiv: 0807.1896(2008)

[28] Guanghan Cao, Cao Wang, Zengwei Zhu, Shuai Jiang, Yongkang Luo, Shun Chi, Zhi Ren, Qian Tao, Yuetao Wang and Zhu'an Xu.. Superconductivity induced by cobalt doping in iron-based oxyarsenides: arXiv:0807.1304(2008)

[29] Jun Sung Kim , Seunghyun Khim, Liqin Yan, N. Manivannan, Yong Liu, Ingyu Kim, G. R. Stewart, and Kee Hoon Kim . Evidence for co existance of superconductivity and Magnetism in single crystals of Co doped $SrFe_2As_2$ arXiv: 0812.2091v1.

[30] Anupam, P L Paulose, H S Jeevan, C Geibel, and Z Hossain. Interplay between superconductivity and magnetismin K-doped EuFe2As2. arXiv:0812.1131v1.

[31] Efstratios Manousakis, Jun Ren3, Sheng Meng and Efthimios Kaxiras. Is the nature of magnetic order in copper-oxides and in ironpnictides different?: arXiv:0902.3450v1 (2009)

[32] Hiroki Takahashi, Kazumi Igawa, Kazunobu Arii, Yoichi Kamihara, Masahiro Hirano & Hideo Hosono. Superconductivity at 43 K in an iron-based layered compound $LaO_{1-x}F_xFeAs$. Nature 453, 376 (2008).

[33] C. W. Chu and B. Lorenz. High Pressure Studies on Fe-Pnictide Superconductors. arXiv0902.0809iv:

[34] Gang Mu, Huiqian Luo, Zhaosheng Wang, Lei Shan, Cong Ren and Hai-Hu Wen. Fully Gapped Superconducting State Based on a High Normal State Quasiparticle Density of States in $Ba_{0.6}K_{0.4}Fe_2As_2$ Single Crystals: arXiv: 0808.2941.

[35] Hideto Fukazawa, Kenji Hirayama, Kenji Kondo, Takehiro Yamazaki, Yoh Kohori, Nao Takeshita, Kiichi Miyazawa, Hijiri Kito, Hiroshi Eisaki, Akira Iyo. 75As NMR study of the ternary iron arsenide $BaFe_2As_2$:arXiv: 0806.4514

[36] I. A. Nekrasov, Z. V. Pchelkina, M. V. Sadovskii. Electronic Structure of Prototype AFe2As2 and ReOFeAs High-Temperature Superconductors: a Comparison: arXiv:0806.2630.

[37] Hai-Jun Zhang, Gang Xu, Xi Dai and Zhong Fang. Enhanced Orbital Degeneracy in Momentum Space for LaOFeAs: arXiv:0803.4487.

[38] Dirk Johrendt, and Rainer Pöttgen Superconductivity, magnetism and crystal chemistry of $Ba_{1-x}K_xFe_2As_2$.

[39] Tadashi C. Ozawa, Susan M. Kauzlarich. Chemistry of layered d-metal pnictide oxides and their potential as candidates for new superconductors: arXiv:0808.1158.

[40] H.-H. Klauss, H. Luetkens, R. Klingeler, C. Hess, F.J. Litterst, M. Kraken,M.M. Korshunov, I. Eremin, S.-L. Drechsler, R. Khasanov, A. Amato, J. Hamann-Borrero, N. Leps, A. Kondrat, G. Behr, J. Werner, and B. B¨uchner. Commensurate Spin Density Wave in LaFeAsO: A Local Probe Study arXiv:0805.0264

[41] Spin Ordering in LaOFeAs and Its Suppression in Superconductor LaO0.89F0.11FeAs Probed by Mossbauer Spectroscopy: arXiv:0805.0041

[42] Diploma thesis Mathias Weiler.TUM: Magnetization control in multiferroic heterostructures.

[43] W. Yu, A. A. Aczel, T. J. Williams, S. L. Bud'ko, N. Ni, P. C. Canfield, and G. M. Luke,: The Absence of Superconductivity in Single Phase CaFe2As2 under Hydrostatic: arxiv:0811.2554 (2008).

[44] K. Haule, J. H. Shim, and G. Kotliar. Correlated electronic structure of LaO1-xFxFeAs: arXiv:0803.1279

[45] C. Liu, G. D. Samolyuk, Y. Lee, N. Ni, T. Kondo,,A. F. Santander-Syro,,S. L. Bud'ko, J. L. McChesney, E. Rotenberg, T. Valla, A. V. Fedorov, P. C. Can_eld, B. N. Harmon, and A. Kaminski. The Fermi surface of Ba1-xKxFe2As2 and its evolution with doping: arXiv: 0806.3453

[46] G. L. Sun, D. L. Sun, M. Konuma, P. Popovich, A. Boris, J. B. Peng,K.-Y. Choi, P. Lemmens and C. T. Lin. Iron pnictides: Single crystal growth and effect of doping on structural, transport and magnetic properties: arXiv:0901.2728.

[47] Yu-Zhong Zhang, Hem C. Kandpal, Ingo Opahle, Harald O. Jeschke, and Roser Valent Microscopic origin of pressure-induced phase transitions in iron-pnictide AFe2As2 superconductors: an ab initio molecular-dynamics study: arXiv:0812.2920v1.

[48] N. Ni, M. E. Tillman, J.-Q. Yan,A. Kracher, S. T. Hannahs, S. L. Bud'ko, and P. C. Canfield.Effects of Co substitution on thermodynamic and transport properties and anisotropic Hc2 in Ba(Fe1-xCox)2As2 single crystals: arXiv:0811.1767

[49] L. Boeri, O.V. Dolgov, and A.A. Golubov: Is $LaO_{1-x}F_xFeAs$ an electron-phonon superconductor ?:arXiv:0803.2703v1.

[50]Jun Dai, Zhenyu Li, Jinlong Yang, and J. G. Hou : A first principles study on the electronic and magnetic properties of Ba1−xKxFe2As2: arXiv.0808.0065v1.

[51]T. Goko, A. A. Aczel, E. Baggio-Saitovitch, S. L. Bud'ko, P.C. Canfield, J. P. Carlo, G. F. Chen, Pengcheng Dai, A. C. Hamann, W. Z. Hu, H. Kageyama, G. M. Luke, J. L. Luo, B. Nachumi, N. Ni, D. Reznik, D. R. Sanchez-Candela, A. T. Savici, K. J. Sikes, N. L. Wang, C. R. Wiebe, T. J. Williams, T. Yamamoto,9 W. Yu, and Y. J. Uemura: Superconductivity coexisting with phase-separated static magnetic order in (Ba,K)Fe2As2, (Sr,Na)Fe2As2 and CaFe2As2: 0808.1425v1

[52] J. K. Dong, L. Ding, H. Wang, X. F. Wang, T. Wu, X. H. Chen, and S. Y. Li : Thermodynamic properties of Ba1-xMxFe2As2 (M = La and K): arXiv:0806.3573

Acknowledgments

8. Acknowledgments

I would like to express my appreciation to my advisor Prof Dr. Rudolf Gross for giving me an opportunity to be a part of the WMI research team.

Dr. Adreas Erb, thank you very much for sharing your valuable time on various questions, introducing all the experiments related to this work and giving me a room to work independently. Without your interaction and support, I could not be able to reach at this stage.

I would like to acknowledge Mathias Althamer, Franz Czeschka, and Toni Helm for their respective contributions to the research both in experimental and theoretical way.

I also would like to thank Karen Helm Knapp and Astrid Habel for their help and cooperation during the experiments and sharing their offices with me.

I also would like to thank all the colleagues at Walther Meissner Insitute who helped me to finish this work successfully.

My deepest appreciation goes to my husband, I would have never come so far without him and I am extremely thankful to my parents for everything they have ever done for me.